Global Correlation analysis of strongly nonlinear frequency responses using the Arclength-based separation and the Correlation-map

Zhu Tianxu , Zhang Genbei , Zang Chaoping , M.I. Friswell

PII: S0022-460X(23)00447-9
DOI: https://doi.org/10.1016/j.jsv.2023.117998
Reference: YJSVI 117998

To appear in: *Journal of Sound and Vibration*

Received date: 31 December 2022
Revised date: 23 July 2023
Accepted date: 7 August 2023

Please cite this article as: Zhu Tianxu , Zhang Genbei , Zang Chaoping , M.I. Friswell , Global Correlation analysis of strongly nonlinear frequency responses using the Arclength-based separation and the Correlation-map, *Journal of Sound and Vibration* (2023), doi: https://doi.org/10.1016/j.jsv.2023.117998

Highlights

- Correlation analysis of strongly nonlinear frequency responses is proposed
- Correlation functions with complex multivalued behavior are computed
- Real and fake correlations within the multivalued responses are extracted
- Correlation analysis is conducted for responses with different multivalued behavior

Global Correlation analysis of strongly nonlinear frequency responses using the Arclength-based separation and the Correlation-map

Zhu Tianxu[1], Zhang Genbei[1], **Zang Chaoping[1]***, Friswell. M.I[2]

E-mail: c.zang@nuaa.edu.cn

(1. College of Energy and Power Engineering, Nanjing University of Aeronautics and Astronautics, Nanjing 210016, China)

(2. Department of Aerospace Engineering, Swansea University, Swansea SA1 8EN, United Kingdom)

Abstract: Global correlation analysis is an important technique to quantify both the shape and amplitude differences between two response vectors. In linear dynamic systems, differences between two Frequency Response Functions (FRFs) are quantified as scalar number curves of the Global Shape Criterion (GSC) and the Global Amplitude Criterion (GAC), to represent FRF similarities at different frequencies. From linear to nonlinear, responses are usually obtained at different frequencies to form the Frequency Response Curve (FRC), replacing the FRF for dynamic analysis. Extending the concept of global correlation analysis from linear FRFs to nonlinear FRCs could quantify shape and amplitude similarities between nonlinear models. However, global correlation analysis for multivalued FRCs with a strong nonlinearity is hard to conduct, as strongly nonlinear correlation functions have complex multivalued phenomena with real/fake characteristics. In this paper, the Global Shape Curve Criterion (GSCC) and Global Amplitude Curve Criterion (GACC) are proposed for the correlation analysis of strongly nonlinear FRCs, which can quantify the similarity between two FRCs with different and complex multivalued phenomena. Through the arclength-based separation, multivalued FRCs are separated to single-valued response branches, in order to compute single-valued correlation functions that form the multivalued correlation function. The computed correlations contain the GSCC and GACC, which separately represent shape and amplitude differences between two FRCs at each frequency. The multivalued correlation function is represented as a Correlation-Map (C-MAP) to extract real correlation characteristics, for accurate correlation analysis. The multivalued correlation analysis is first verified on a 3 DOF model with a strong nonlinearity. Differences between the reference and initial multivalued FRCs are successfully quantified as scalar curves and the GACC may be more sensitive than the GSCC on models with a local nonlinearity. Then, the proposed method is further validated on an experimental 3 DOF model. Very complex 15-valued correlation functions between FRCs with different multivalued phenomena are established. Even so, the real correlations are still successfully extracted by the C-MAP. These show the validity and superiority of the proposed method.

Keywords: Multivalued correlation function; Multivalued frequency response curve; Strong nonlinearity; Correlation-map; Arclength-based separation

Symbol list

Symbol	descriptions
$\boldsymbol{H}$	FRF

χ_s	GSC
χ_a	GAC
$\boldsymbol{X}$	FRC
γ_s	GSCC
γ_a	GACC
$\boldsymbol{A}$	Amplitude
$\boldsymbol{P}$	Phase
$\boldsymbol{S}$	Arclength
ω	Frequency
F_{ex}	Force
$\boldsymbol{M}$	Mass matrix
$\boldsymbol{C}$	Damping matrix
$\boldsymbol{K}$	Stiffness matrix
$\boldsymbol{u}$	Displacement response vector
k_i^o	Nonlinear stiffness with the odd order (numerical case)
$\boldsymbol{N}_i^{ko}$	Position matrix with the odd order (numerical case)
p_i^o	Order of the odd polynomial stiffness
k_{odd}^i	Nonlinear stiffness with the odd order (experimental case)
k_{even}^i	Nonlinear stiffness with the even order (experimental case)
N_{kodd}^i	Position matrix of the odd order nonlinear stiffness (experimental case)
$\boldsymbol{N}_{keven}^i$	Position matrix of the even order nonlinear stiffness (experimental case)
$\boldsymbol{k}_{nl}$	Vector of the whole nonlinear stiffness
$\odot$	Kronecker product
$sign$	Signature function

1. Introduction

Correlation functions [1] are an important tool to quantify the extent of the differences between two sets of data in structural dynamics. It is widely used in engineering applications such as model validation [2], damage detection [3], structure health monitoring (SHM) [4], etc.

In linear dynamic systems, the Natural Frequency Difference (NFD) [1] is compared after a set of Correlated Mode Pairs (CMPs) are identified between the experimentally-derived model and the analytical or predicted model. Comparison of mode shapes is mostly carried out by the Modal Assurance Criterion (MAC)[5] and the Coordinate MAC (CoMAC)[6]. The correlation of response properties depends on the form of the response functions, for example, Frequency Response Functions (FRFs) or sometimes Operating Deflection Shapes (ODSs). Similar to the MAC approach, the Frequency Domain Assurance Criterion (FDAC) [7] was defined to compare the large number of frequencies with the number of modes in the concerned frequency range. Equivalent to the CoMAC, the Frequency Response Assurance Criterion (FRAC) [8] was also defined to provide the frequency amplitude-based information in the spatial domain. The most useful correlations are perhaps the Global Shape Criterion (GSC) and Global Amplitude Criterion (GAC)[9] because they can quantify the overall agreement of both shape and amplitude information between two models as a function of frequency. In order to compare the experimental ODS properties at the measured resonance frequencies with the analytical model mode shapes, the hybrid correlation, called the mode-response correlation (MFAC), was also defined [1].

From linear to nonlinear, it is hard to obtain the characteristic equation [10] from the nonlinear system, to solve modal frequencies to obtain modal vectors. Hence, the concept of linear modes, or the Linear Normal Mode (LNM), cannot be to be applied to nonlinear systems. Instead, the concept of the Nonlinear Normal Mode (NNM) [11][12] was developed for nonlinear analysis. However, NNMs are energy dependent and they are usually represented as the Frequency-Energy Plot (FEP) [13], to extract the Back-Bone Curves (BBCs) for nonlinear analysis, which are very different from the LNMs. Currently, using the traditional modal correlation function, such as the MAC, for the correlation analysis of the FEPs or the BBCs is less reported. For the nonlinear response properties, FRFs[14] cannot be obtained through the superposition of modal properties and vary as the force level increases, but also loses its meaning which assumes linearity. Instead, responses at different frequencies are usually measured [15] or predicted [16] through sinusoidal excitations, to obtain the Frequency Response Curves (FRCs) for the nonlinear analysis. Hence, the objective of correlation analysis for nonlinear response properties changes from FRFs to FRCs. The FRC is force dependent, and its properties vary from weakly nonlinear to strongly nonlinear, as the excitation level increases. The weakly nonlinear FRC [17] for low force levels is similar to the FRF, and they are both single-valued functions with respect to the excitation frequency. Hence, response correlation techniques for weak nonlinearities can be developed from the FRF correlation functions.

However, the strongly nonlinear FRC [18] for high force levels exhibits multivalued phenomenon induced by bifurcation behavior. Several responses exist at an excitation frequency, which is very different from the linear FRF. Some of the traditional FRF correlation functions, such as the FDAC [19][20], can still be applied to the multivalued FRCs. All the response points on two multivalued FRCs are used to establish the matched response pairs, to quantify the response closeness. The FDAC is a shape-based method, and two FRCs for some locally nonlinear

structures may rarely show shape differences and hence shape-based correlation techniques work badly. In contrast, global correlation techniques, such as the GSC and GAC, can distinguish both shape and amplitude differences as a function of frequency, which may be more appropriate for developing strongly nonlinear correlation techniques. However, global correlation analysis for multivalued FRCs results in very complex multivalued correlation curves that are hard to compute. Within a multivalued global correlation function, only real regions can represent the correct differences between the FRCs, whereas the remaining are fake and meaningless. These properties restrict the successful implementation of a global correlation analysis on strongly nonlinear systems. Hence, it is important to study techniques of the multivalued correlation computation and real correlation selection, for strongly nonlinear global correlation analysis.

Once the above mentioned multivalued global correlation analysis is established, such a technique could be applied to the multivalued FRCs predicted from the theoretical model and measured from the real nonlinear structure. At each frequency, the differences between the predicted and measured multivalued responses can be quantified as several real correlation functions, where each real correlation function is a scalar number. The quantified real correlation functions at different frequencies could form two multivalued scalar number curves, separately representing the shape and amplitude differences between the FRCs. Then, as the real correlation functions represent the correct differences between the FRCs, the two multivalued correlation curves will be the unit, when the predicted and measured FRCs are fully correlated. The quantified real correlation function curves may be very helpful for the further nonlinear analysis, such as model updating of the strongly nonlinear structures using the multivalued responses. Accordingly, strongly nonlinear model updating perhaps could be implemented using the linear FRF correlation updating framework, which will be convenient to construct the accurate strongly nonlinear model for applications in aeras of strongly nonlinear structural model validation and damage detection, etc.

In this paper, the Global Shape Curve Criterion (GSCC) and the Global Amplitude Curve Criterion (GACC) considering both the frequency responses and the level of the excitation force are proposed for the correlation analysis of two data sets with a strong nonlinearity in the frequency domain. Through the arclength coordinate, the multivalued FRCs are first separated into a set of single-valued branches and single-valued correlation functions are computed between the branches on two FRCs. Superposing the computed correlations in one figure results in the complete multivalued correlation function curves of the shape and amplitude. Then, a Correlation-Map (C-MAP) that represents the multivalued correlation function curves is built to judge the real and fake correlation characteristics, to extract the real region for an accurate analysis. This technique can quantify both the shape and amplitude differences between two FRCs with different and complex multivalued phenomena. The multivalued correlation analysis is conducted on a numerical 3 DOF nonlinear system for verification and further conducted on an experimental 3 DOF system for validation.

The rest of the paper is arranged in five sections. In Section 2, the multivalued correlation function and the problems encountered are described generally. Section 3 outlines the main format of the global correlation analysis. In Section 4, the multivalued correlation analysis is applied to a numerical 3 DOF system with a strong nonlinearity and applied to an experimental 3 DOF system with a strong nonlinearity in Section 5. Conclusions are drawn in the last section.

2. Correlation functions of Frequency Response Curves

In linear dynamic systems, the FRFs are force independent. Accordingly, the developed global correlation techniques, namely Global Shape Criterion (GSC) and Global Amplitude Criterion (GAC), are also force independent, and hence are only functions of frequency. Thus

$$\chi_s(\omega)=\frac{\left|\left\{\boldsymbol{H}_{measure}(\omega)\right\}^H\left\{\boldsymbol{H}_{predict}(\omega)\right\}\right|^2}{\left(\left\{\boldsymbol{H}_{measure}(\omega)\right\}^H\left\{\boldsymbol{H}_{measure}(\omega)\right\}\right)\left(\left\{\boldsymbol{H}_{predict}(\omega)\right\}^H\left\{\boldsymbol{H}_{predict}(\omega)\right\}\right)} \tag{1}$$

$$\chi_a(\omega)=\frac{2\left|\left\{\boldsymbol{H}_{measure}(\omega)\right\}^H\left\{\boldsymbol{H}_{predict}(\omega)\right\}\right|}{\left(\left\{\boldsymbol{H}_{measure}(\omega)\right\}^H\left\{\boldsymbol{H}_{measure}(\omega)\right\}\right)+\left(\left\{\boldsymbol{H}_{predict}(\omega)\right\}^H\left\{\boldsymbol{H}_{predict}(\omega)\right\}\right)} \tag{2}$$

where χ_s and χ_a are global correlation functions between the predicted and measured FRFs. The subscripts '*s*' and '*a*' separately denote 'shape' and 'amplitude'. $\boldsymbol{H}$ denotes the FRF vector and the superscript '*H*' is the complex conjugate transpose. The above equations represent that, at the frequency ω, the shape and amplitude differences between the predicted and measured FRF vectors are quantified as two scalars between 0 and 1, where the correlation function close to the identity denotes that two FRFs are close. After correlation functions are established at individual frequencies, two frequency correlation curves are obtained to globally represent the difference between two FRFs. A schematic diagram is given in Fig. 1.

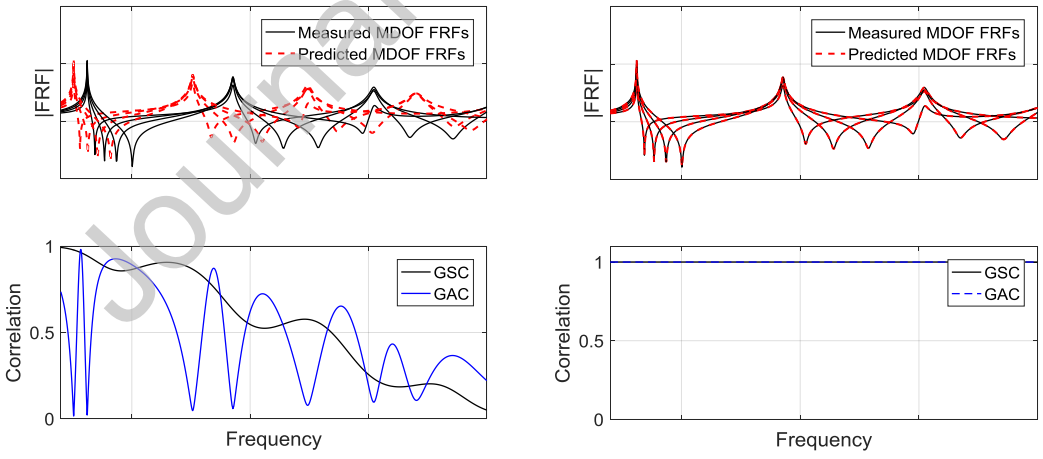

(a) Correlation function (Large difference) (b) Correlation function (Fully correlated)

Fig. 1 Schematic diagram of the correlation function curves for linear FRFs

Fig. 1(a) gives correlation functions between the predicted and measured FRFs with a relatively large difference, where the resonance frequencies for the two FRFs vary widely. Differences between two FRFs are quantified as two correlation curves. Each curve is formed by scalars between 0 and 1 that denote the shape or amplitude difference between the predicted and measured FRFs at all DOFs, instead of a single DOF. When the predicted and measured FRFs are

the same and fully correlated, the related correlation functions are schematically given in Fig. 1(b). It is clear that both the GSC and GAC curves are equal to unity at all frequencies.

As the system turns from linear to nonlinear, the superposition principle no longer applies to the nonlinear system and FRFs [14] cannot be deduced through the modal properties. Nonlinear FRFs are no longer force independent and vary as the force level increases. Due to the existence of higher harmonic terms, it usually needs to strictly define the nonlinear FRFs through the Volterra series and the results are very complex. Hence, the FRF may gradually lose its meaning for the nonlinear system.

The response itself is usually used to replace the FRF for nonlinear analysis in the frequency domain. Under sinusoidal excitations, the nonlinear computed and experimentally measured responses for different frequencies and forces, are used to form the Frequency Response Curves (FRCs) under constant force levels for nonlinear identification [15], nonlinear model updating [17], etc. A schematic diagram of the amplitude of the FRC is given in Fig. 2. For a low force level, the FRC shows a weak nonlinearity and is a single-valued function with respect to frequency, which is similar to the FRF. For a high force level, the FRC shows a strong nonlinearity and is still the function of frequency, but its resonance region shifts to the right compared to the weakly nonlinear FRC and contains a multivalued region determined by the bifurcation frequencies.

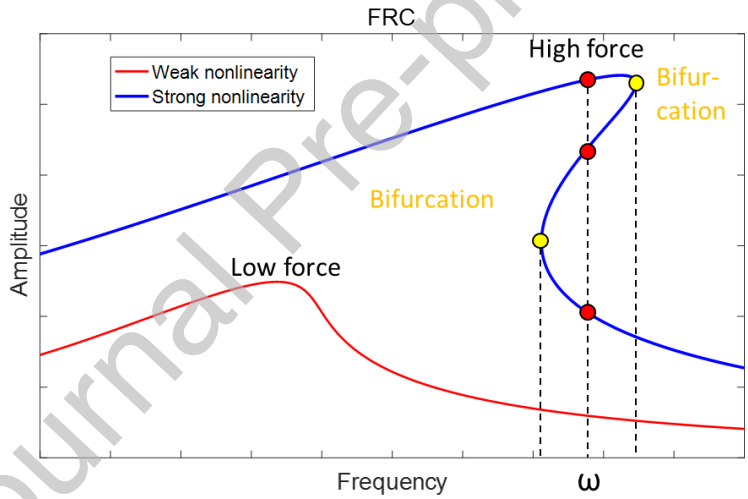

Fig. 2 Schematic diagram of the amplitude of FRCs

The FRC is still a function of frequency. Hence, global correlation analysis for FRCs can be deduced from the GSC and GAC technique. However, FRCs contain different frequency properties under different force levels. Accordingly, the correlation functions for FRCs should be force dependent. Under these concepts, the Global Shape Curve Criterion (GSCC) and Global Amplitude Curve Criterion (GACC) are derived for the global correlation analysis of FRCs as:

$$\gamma_s(\omega,F_{ex})=\frac{\left|\left\{\boldsymbol{X}_{measure}(\omega,F_{ex})\right\}^H\left\{\boldsymbol{X}_{predict}(\omega,F_{ex})\right\}\right|^2}{\left(\left\{\boldsymbol{X}_{measure}(\omega,F_{ex})\right\}^H\left\{\boldsymbol{X}_{measure}(\omega,F_{ex})\right\}\right)\left(\left\{\boldsymbol{X}_{predict}(\omega,F_{ex})\right\}^H\left\{\boldsymbol{X}_{predict}(\omega,F_{ex})\right\}\right)} \tag{3}$$

$$\gamma_a(\omega,F_{ex})=\frac{2\left|\left\{\boldsymbol{X}_{measure}(\omega,F_{ex})\right\}^H\left\{\boldsymbol{X}_{predict}(\omega,F_{ex})\right\}\right|}{\left(\left\{\boldsymbol{X}_{measure}(\omega,F_{ex})\right\}^H\left\{\boldsymbol{X}_{measure}(\omega,F_{ex})\right\}\right)+\left(\left\{\boldsymbol{X}_{predict}(\omega,F_{ex})\right\}^H\left\{\boldsymbol{X}_{predict}(\omega,F_{ex})\right\}\right)} \quad (4)$$

where γ_s and γ_a are the GSCC and the GACC. They separately denote the global shape differences and global amplitude differences for the FRCs. The formulations of γ_s and γ_a are the same as the formulations of χ_s and χ_a. However, comparing with χ_s and χ_a, the response vector used for correlation analysis changes from the FRF $\boldsymbol{H}$ to the FRC $\boldsymbol{X}$. Furthermore, γ_s and γ_a are not only functions of frequency, but are also functions of the force amplitude. A schematic diagram of the GSCC and GACC is given in Fig. 3.

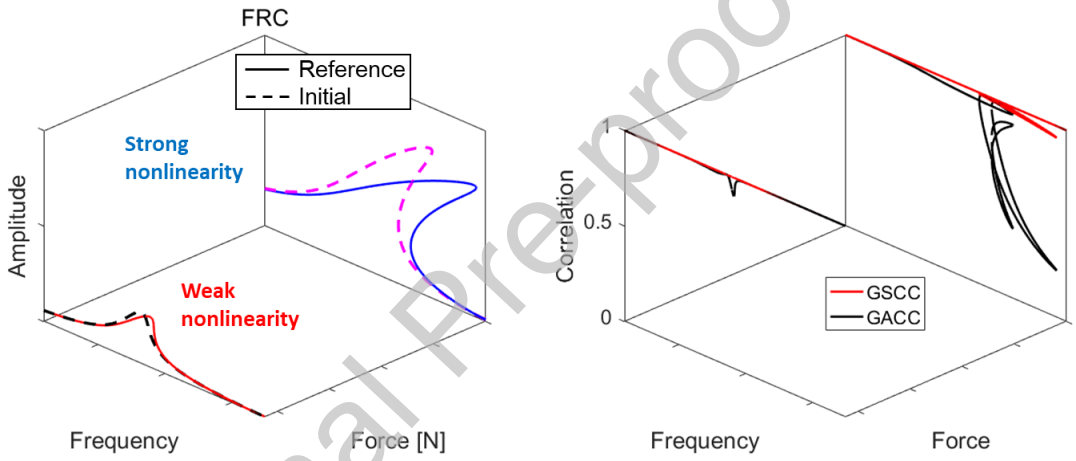

(a) Weakly and strongly nonlinear FRCs (b) Multivalued correlation functions of the FRCs

Fig. 3 Schematic diagram of nonlinear responses and correlation functions

Fig. 3 gives GSCCs and GACCs between the reference (measured) and initial (predicted) FRCs for two models with the different nonlinear parameters. To highlight the differences in the responses, only FRCs at a single DOF are given, instead of the whole set of DOFs. For the low excitation level, where the nonlinearity is weakly excited, the two FRCs are very close and single-valued. Hence, the related correlation functions are single-valued and close to 1. For the high excitation level, where the system nonlinearity is strongly excited, the FRCs become multivalued and the differences between the FRCs increase significantly. Meanwhile, the correlation analysis induces multiple values and the calculated correlation function curves are multivalued.

However, the multivalued phenomenon of the correlation function for the high force level is very complex. The related GACC curve is extracted for exploring its multivalued behavior and the result is given in Fig. 4.

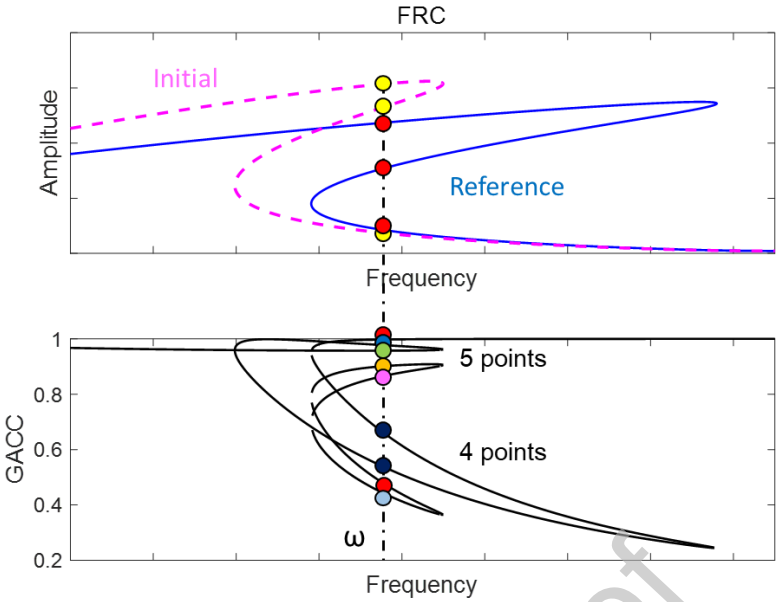

Fig. 4 Multivalued GACC curve between the reference and initial multivalued FRCs

Fig. 4 gives the multivalued GACC between the multivalued reference and initial FRCs. At the frequency ω, both the reference and initial FRCs contain three response points. On the related GACC curve, nine values exist at ω. This indicates that the number of the correlation functions at each frequency is the product of the numbers of the predicted and measured responses. Thus

$$N_{correlation} = N_{response}^{predict} \times N_{response}^{measure} \tag{5}$$

and, in the multivalued regions of the responses, the number of correlation functions is typically much higher than the number of responses. Accordingly, the multivalued phenomenon of the correlation function curve is more complex than the response phenomenon, which indicates that the computation of the multivalued correlation function may be difficult.

The property, $N_{correlation} > N_{response}$, also reveals that the multivalued correlation function may contain the real and fake parts. The real and fake correlation functions can be easily seen when correlation functions are established between two multivalued FRCs that are fully correlated. The related schematic diagram is given in Fig. 5.

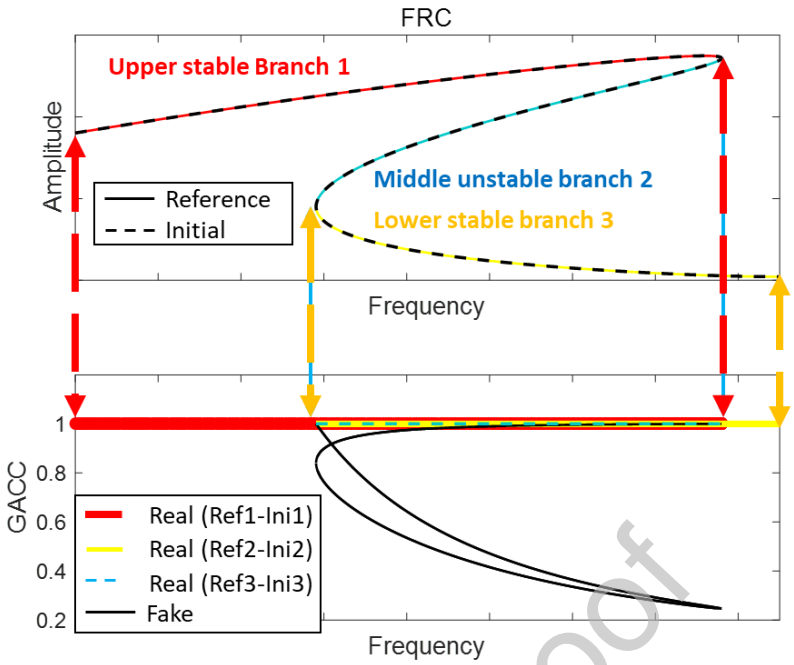

Fig. 5 Schematic diagram of the correlation function (FRC fully correlated)

Fig. 5 gives the GACC curve between two identical FRCs. The reference and initial FRCs are treated as upper stable branches, middle unstable branches and lower stable branches, labelled as 1, 2 and 3. As the two FRCs are fully correlated, the generated GACC curve should be equal to unity. However, only GACCs between the reference and initial FRC branches with the same labels are equal to 1 and denote the real amplitude differences. The remainder of the GACC curves are between FRC branches with different labels and are lower than 1. They are likely to be fake and meaningless, and should be excluded for an accurate correlation analysis.

To sum up, the global correlation analysis for multivalued FRCs has two main issues to be solved:

- How to compute the multivalued GSCC and GACC curves that contain much more complex multivalued behavior compared with the FRCs.
- How to divide the real and fake correlation characteristics within the multivalued correlation function curve and select the real region for an accurate correlation analysis.

3. Multivalued correlation analysis using Arclength-based separation and Correlation-Map

The multivalued correlation analysis using Arclength-based separation and the Correlation-Map (C-MAP) is proposed, for the computation of correlation functions between multivalued FRCs and the selection of the real parts for an accurate correlation analysis. The technique is divided mainly into three steps. Step 1 is the separation of the multivalued FRCs into single-valued response branches using our previously proposed Arclength-based separation

technique [21]. The multivalued FRC is parameterized by the separate parameter arclength obtained during continuation, resulting in single-valued arclength response curves. The response separation is then conducted on the arclength coordinate and the separation results are transformed back to the frequency coordinate to form the single-valued FRC branches. Step 2 is the computation of the multivalued correlation function curve. The single-valued correlation function curves are constructed between two arbitrary FRC branches of the prediction and measurement, which may be superposed to form a complete curve of the multivalued correlation function. Step 3 is the selection of the real part from the multivalued correlation function for an accurate correlation analysis. The single-valued correlation functions are used to form a Correlation-Map (C-MAP) to select the real correlation functions. The above steps may be summarized in the flow chart shown in Fig. 6.

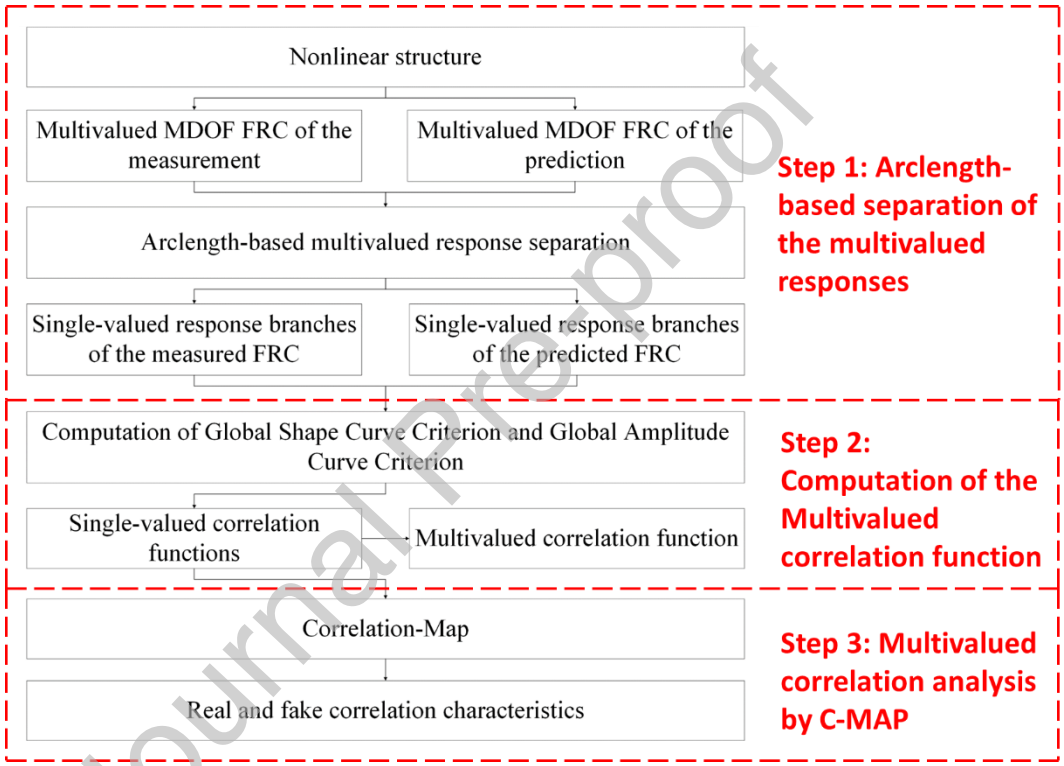

Fig. 6 Schematic diagram of the multivalued correlation analysis

3.1 Arclength-based response separation of the multivalued responses

The response separation of the multivalued FRC into a set of single-valued branches is an important step for the computation of the multivalued correlation function, as the correlation function curves assume single-valued responses. Our previously proposed arclength-based response separation is used to divide the multivalued FRC. Arclength is the independent parameter in the continuation process for parameterizing the frequency responses. Accordingly, multivalued FRCs could be represented as single-valued functions with respect to arclength. The single-valued arclength responses could be easily separated into a set of branches through their feature points. Extracting the FRCs from these separated branches, the results are single-valued responses with respect to the excitation frequency.

First, a schematic diagram of the 3 DOF FRC with the multivalued phenomenon obtained from the response prediction or measurement is shown in Fig. 7. The FRC is a complex response curve with the real and imaginary parts. Using the polar coordinate, its amplitude and phase can be extracted:

$$\boldsymbol{X} = \boldsymbol{A} * e^{i \times \boldsymbol{P}} \tag{6}$$

where $\boldsymbol{A}$ is the amplitude vector and $\boldsymbol{P}$ is the phase vector. For each DOF, the amplitude of the multivalued FRC contains the response peak and the response bifurcations as its feature points, and these feature points can be used to divide the multivalued curve to single-valued branches. However, the extraction of the feature points and the response separation are hard to conduct directly on the multivalued curve due to the processing difficulty.

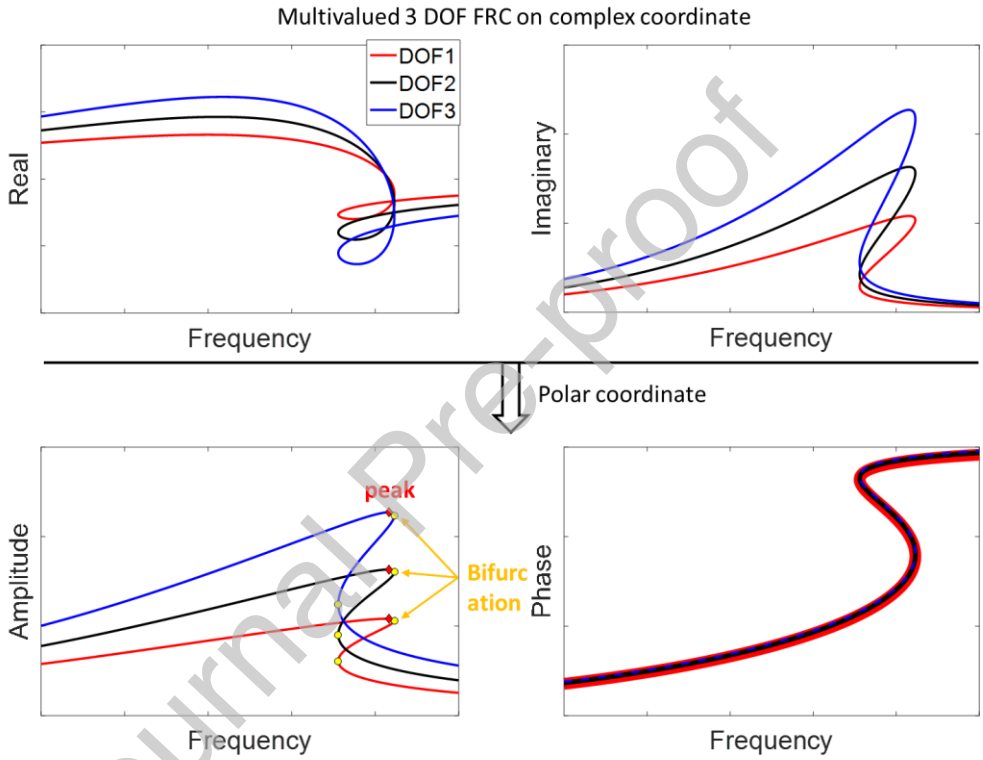

Fig. 7 Multivalued 3 DOF FRC on two coordinates and FRC feature points

During the prediction of multivalued responses using the continuation scheme, arclength Δs is a positive value to control the distance between adjacent points on the FRCs. The arclength vector $\boldsymbol{s}$ gives the accumulation of arclength parameters Δs related to the computed responses:

$$\Delta s = \sqrt{\left|\Delta \boldsymbol{A}\right|^2 + \Delta\omega^2} \qquad \boldsymbol{s} = \left\{0 \quad \Delta s_1 \quad \sum_{i=1}^{2} \Delta s_i \quad \cdots \quad \sum_{i=1}^{n} \Delta s_i\right\} \tag{7}$$

Monotonically increase

where ω is the excitation frequency. The element of the arclength vector is the accumulation of positive values. Therefore, the elements of the arclength vector monotonically increase as the computation continues. The arclength can then be used to parameterize the FRC:

$$\begin{aligned}\omega &= K(s)\\ \boldsymbol{X} &= L(s)\\ \boldsymbol{A} &= M(s)\end{aligned} \tag{8}$$

The schematic diagram of the Arclength-Amplitude curve is given in Fig. 8(a). It is clear that the 3 DOF curve is no longer multivalued, but a single-valued function with respect to arclength, where arclength s_{peak} related to the maximum peak response may be directly extracted. The Arclength-Frequency curve is given in Fig. 8(b) and similarly, the response curve is single-valued. Frequency extremes on the curve are related to bifurcations and the related arclength parameters are directly extracted as $\boldsymbol{s}_{bif}$.

$$\begin{aligned}&\boldsymbol{s}_{bif} = \left\{ s_{bif}^1 \quad s_{bif}^2 \quad \cdots \quad s_{bif}^m \quad s_{bif}^{m+1} \quad \cdots \quad s_{bif}^{m+n} \right\}\\ &s.t: s_{bif}^m < s_{peak} \quad s_{bif}^{m+1} > s_{peak}\end{aligned} \tag{9}$$

where $\boldsymbol{s}_{bif}$ contains $m+n$ elements related to $m+n$ bifurcation points. The arclength parameters related to the first m bifurcation points are below s_{peak} and the rest of the n arclength parameters are above s_{peak}.

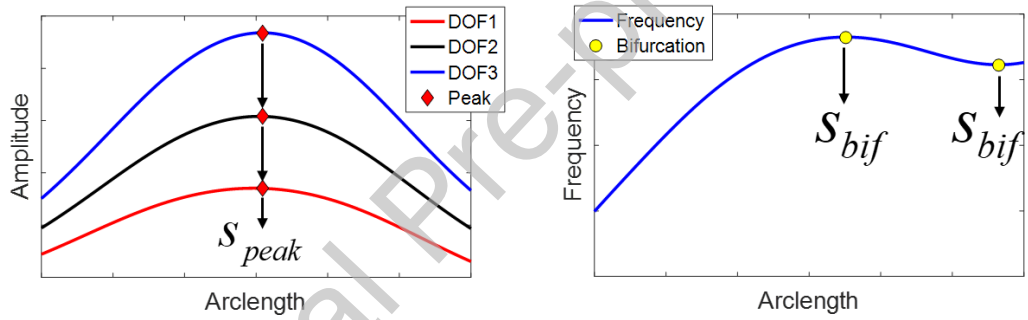

(a) Arclength-Amplitude curve (b) Arclength-Frequency curve

Fig. 8 Schematic diagram of the Arclength-Amplitude and Arclength-Frequency curves

According to the extracted arclength parameters related to the feature points, the response separation is conducted for the arclength parameters, frequencies, FRCs:

$$\begin{aligned}&\qquad\qquad\quad L1 \qquad\qquad\quad L2 \qquad\quad \cdots\\ &lef-separation: \begin{array}{l}\boldsymbol{S} = \{\{s_1 \quad s_2 \quad \cdots \quad s_{bif}^1\} \quad \{\cdots \quad s_{bif}^2\} \quad \{\cdots\} \quad s_{peak}\\ \boldsymbol{\omega} = \{\{\omega_1 \quad \omega_2 \quad \cdots \quad \omega_{bif}^1\} \quad \{\cdots \quad \omega_{bif}^2\} \quad \{\cdots\} \quad \omega_{peak}\\ \boldsymbol{X} = \{\{\boldsymbol{X}_1 \quad \boldsymbol{X}_2 \quad \cdots \quad \boldsymbol{X}_{bif}^1\} \quad \{\cdots \quad \boldsymbol{X}_{bif}^2\} \quad \{\cdots\} \quad \boldsymbol{X}_{peak}\end{array}\\ &\qquad\qquad\quad R1 \qquad\qquad\quad R2 \qquad\quad \cdots\\ &right-separation: \begin{array}{l}\{\{s_{end} \quad s_{end-1} \quad \cdots \quad s_{bif}^{m+n}\} \quad \{\cdots \quad s_{bif}^{m+n-1}\} \quad \{\cdots\} \quad s_{peak}\\ \{\{\omega_{end} \quad \omega_{end-1} \quad \cdots \quad \omega_{bif}^{m+n}\} \quad \{\cdots \quad s_{bif}^{m+n-1}\} \quad \{\cdots\} \quad \omega_{peak}\\ \{\{\boldsymbol{X}_{end} \quad \boldsymbol{X}_{end-1} \quad \cdots \quad \boldsymbol{X}_{bif}^{m+n}\} \quad \{\cdots \quad s_{bif}^{m+n-1}\} \quad \{\cdots\} \quad \boldsymbol{X}_{peak}\end{array}\end{aligned} \tag{10}$$

The above separation means that, from the initial arclength parameter s_1 and the end arclength parameter s_{end}, the arclength parameters together with the related frequencies and FRC vectors are continually labelled as $L1$ and $R1$. As the labelling crosses s_{bif}, the labelled number increases by 1, and branches $L1$ and $R1$ are divided from the whole data. The labelling ends at s_{peak}. The

whole data are separated to m+1 left branches and n+1 right branches. Eliminating arclength, the separated branches of the multivalued FRC may be extracted:

$$\underbrace{\left(\boldsymbol{\omega}_{L1},\boldsymbol{X}_{L1}\right)}_{\boldsymbol{L1}}\ \cdots\ \underbrace{\left(\boldsymbol{\omega}_{Lm+1},\boldsymbol{X}_{Lm+1}\right)}_{\boldsymbol{Lm+1}}\Big|\ \underbrace{\left(\boldsymbol{\omega}_{Rn+1},\boldsymbol{X}_{Rn+1}\right)}_{\boldsymbol{Rn+1}}\ \cdots\ \underbrace{\left(\boldsymbol{\omega}_{R1},\boldsymbol{X}_{R1}\right)}_{\boldsymbol{R+1}} \tag{11}$$

The whole separated branches of a 3 DOF FRC are schematically plotted in Fig. 9. The multivalued FRC is divided to branches L1, R3, R2 and R1. In each branch, the excitation frequency monotonically increases. This monotonous change denotes that each curve is single-valued

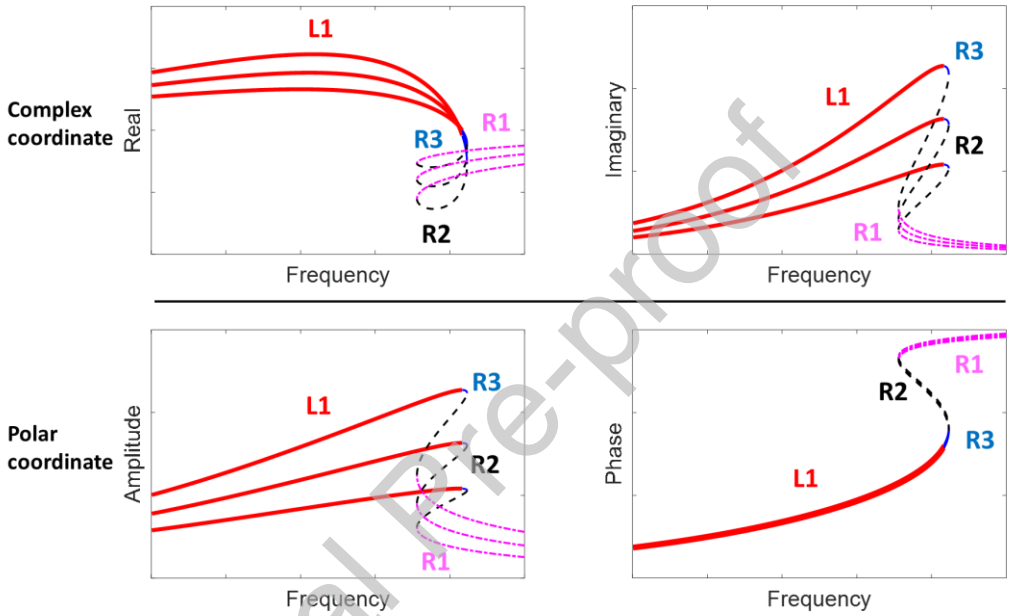

Fig. 9 Separated single-valued response branches on the multivalued 3 DOF FRC

3.2 Computation of the multivalued correlation function curve

After the response separation, the single-valued correlation functions are computed from the separated branches of the predicted and measured FRCs. The computed correlation functions contain the GSCC and the GACC. The GSCC denotes the global shape differences between two FRCs. The GACC denotes the global amplitude differences. By plotting the single-valued correlation functions in one figure, they will superpose to form a complete multivalued correlation function curve.

For arbitrary two branches of the predicted and measured FRC, $\boldsymbol{X}_{measure}$ and $\boldsymbol{X}_{predict}$, the correlation functions may be computed if they contain the same frequency:

$$G\left(\boldsymbol{X}_{measure},\boldsymbol{X}_{predict}\right) \tag{12}$$

where G denotes the correlation computation shown in Eqs. (3) and (4). A related schematic diagram is given in Fig. 10.

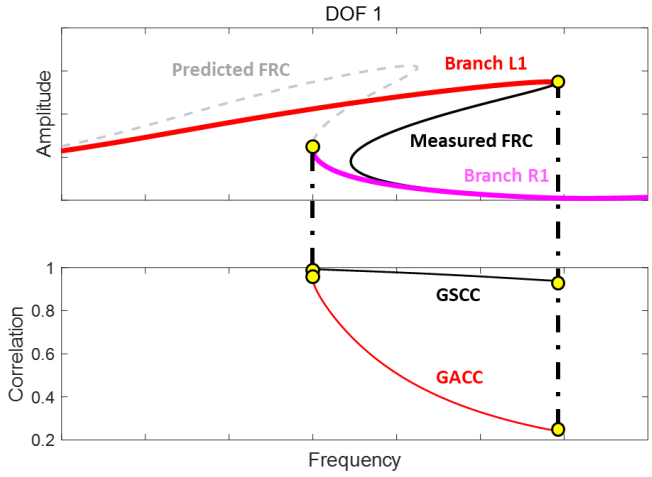

Fig. 10 Schematic diagram of the computation of the single-valued correlation function

Fig. 10 gives the computation of the correlation function curve between the measured response branch L1 and the predicted response branch R1. In the overlapped frequencies of the two branches, both the predicted and measured responses exist and are single-valued, which are directly used for the computation of the correlation functions. The results are the single-valued GSCC and GACC curves, which denote the shape and amplitude differences.

The computed correlation functions are a set of single-valued GSCC and GACC curves, which are shown as:

$$\begin{matrix} \gamma_{s,1} & \gamma_{s,2} & \cdots & \gamma_{s,N} \\ \gamma_{a,1} & \gamma_{a,2} & \cdots & \gamma_{a,N} \end{matrix} \tag{13}$$

The single-valued GACC curves are superposed and schematically plotted in one figure, where the result is given in Fig. 11. In the correlation plot, curves with different colors denote different single-valued GACCs between the FRC branches. It is clear that the superposition of single-valued GACCs is a multivalued correlation function curve. Through the predicted and measured bifurcation frequencies, the whole figure is separated to five parts. In each part, the number of correlations at each frequency is equal to the product of the number of measured responses and the number of predicted responses, which follows Eq. (5). Hence, all of the correlation characteristics are obtained during the correlation computation and the formed correlation curve is complete.

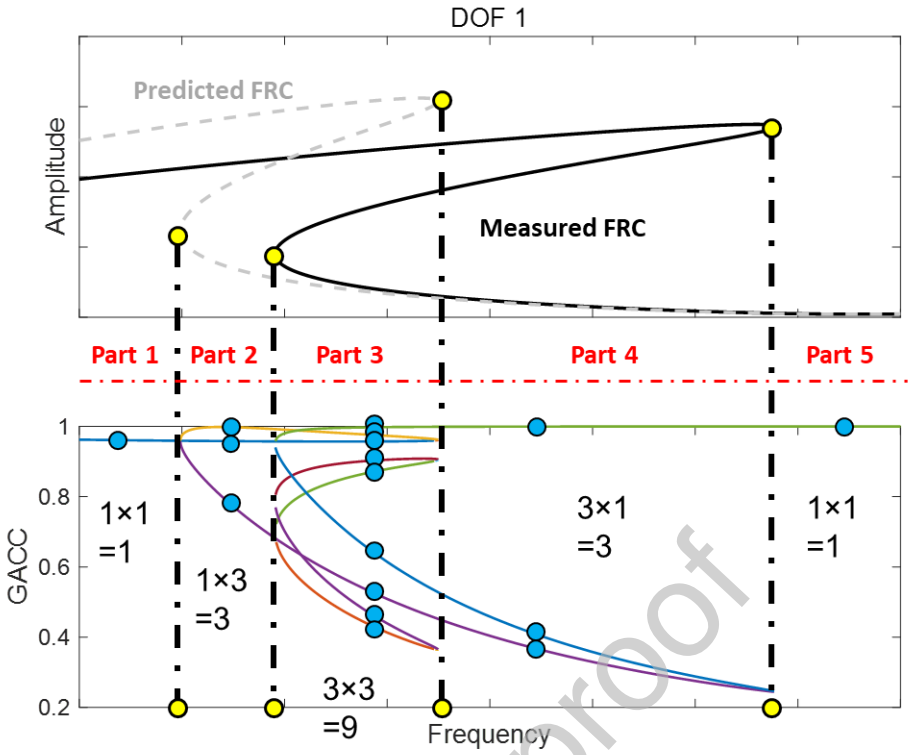

Fig. 11 Schematic diagram of the multivalued correlation function

3.3 Multivalued correlation function analysis by Correlation-Map

After the multivalued correlation function is computed, the fake parts within the computation result should be excluded. A Correlation-Map (C-MAP) is established from the multivalued correlation function to extract the real region. The element of the map is the single-valued correlation function between the separated FRC branches of the measurement and prediction. Using specific rules, real correlation functions may be selected from the elements in the figure and used for accurate correlation analysis.

First, it is hard to directly extract the real parts from the multivalued correlation function, as the related multivalued phenomenon is too complex to be processed. Selecting the real parts from single-valued correlation functions that form the multivalued correlation function may be a better choice. Accordingly, the multivalued correlation function is represented as a C-MAP. The X coordinate of the map is the separated response branches of the prediction and the Y coordinate is the measured branches. The element of the map under the column i and row j denotes the single-valued correlation function between the FRC branch i of the prediction and the FRC branch j of the measurement. Taking the GACC as an example, a schematic diagram of the map is drawn based on the separated branches with the following labels and the result is given in Fig. 12:

$$\begin{aligned} Measure:&\left[L1 \quad R3 \quad R2 \quad R1\right] \\ Predict:&\left[L1 \quad R3 \quad R2 \quad R1\right] \end{aligned} \tag{14}$$

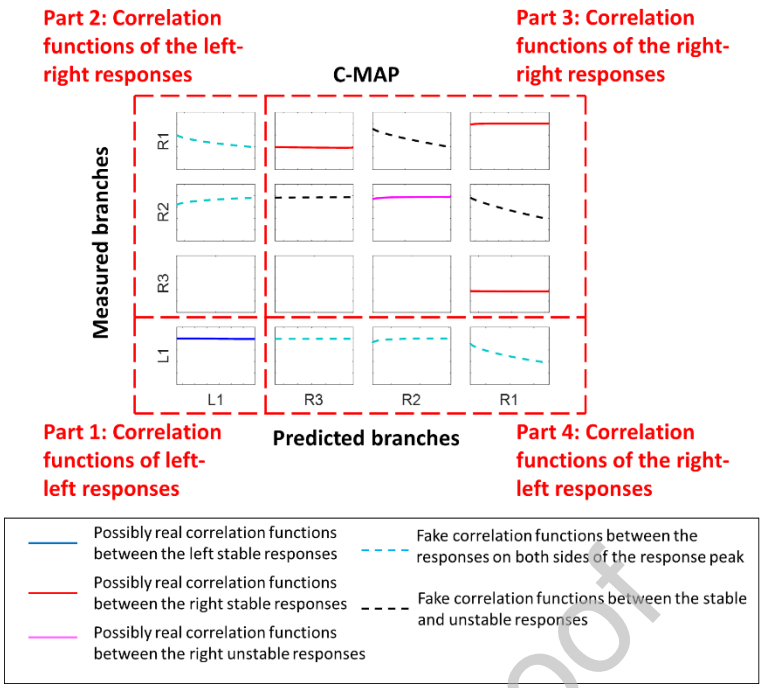

Fig. 12 Schematic diagram of the C-MAP

The map gives 13 single-valued correlation functions between 4 predicted branches and 4 measured branches. From the figure, an initial judgment of the real and fake parts of correlation functions can be made. Based on the response peak, the response separation in Section 3.1 divides the predicted and measured FRCs into left and right branches. According to the left and right branches, the C-MAP could be further separated to four parts. The elements in Part 2 are correlation functions between the left response branches of the prediction and the right response branches of the measurement. The elements in Part 4 are correlation functions between the right branches of the prediction and the left branches of the measurement. These two parts give correlation functions between branches on opposite sides of the response peak. Then, as the predicted FRC gradually converges to the measured FRCs in three iterations, the variation of the Part 4 correlation functions is given in Fig. 13. However, responses on opposite sides of the response peak do not generally coincide with each other. Accordingly, the related correlation function curve is below unity, when two FRCs are fully correlated. Therefore, they are thought to be fake and marked as the dotted lines in light blue.

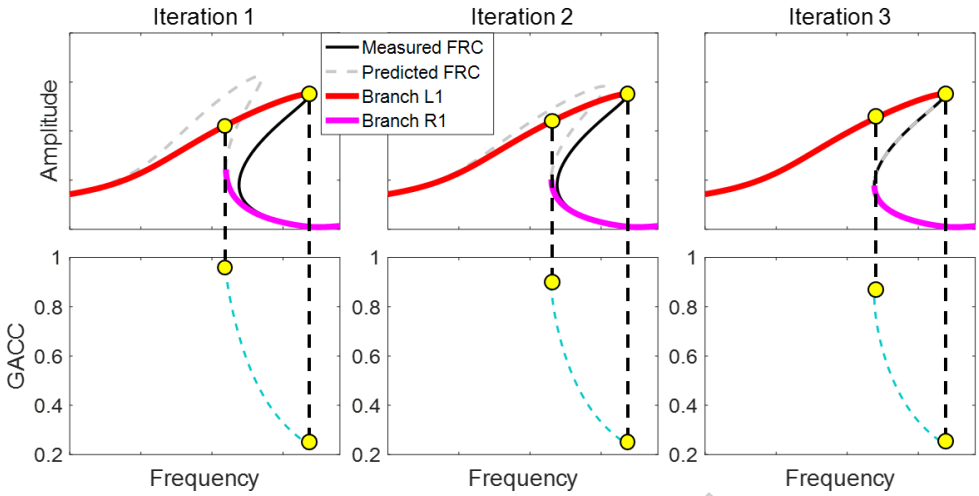

Fig. 13 Schematic diagram of correlation functions on Part 4 of the C-MAP in three iterations

The elements in Part 1 are correlation functions between left branches of the prediction and left branches of the measurement. The elements in Part 3 are correlation functions between right branches of the prediction and right branches of the measurement. Parts 1 and 3 give correlation functions between the branches on the same sides of the response peak. It is judged that real correlation functions are in these two parts. However, the separated branch with an odd number denotes a stable response and the separated branch with an even number denotes an unstable response. The correlation functions between the response branches with odd and even numbers denote correlation functions between the stable and unstable responses. When the predicted FRC converges to the measured FRC from iterations 1 to 3, the variation of such correlation functions is shown in Fig. 14. Stable responses do not converge to unstable responses and the related correlation functions do not converge to unity. Hence, these elements are also fake and marked as black dotted lines.

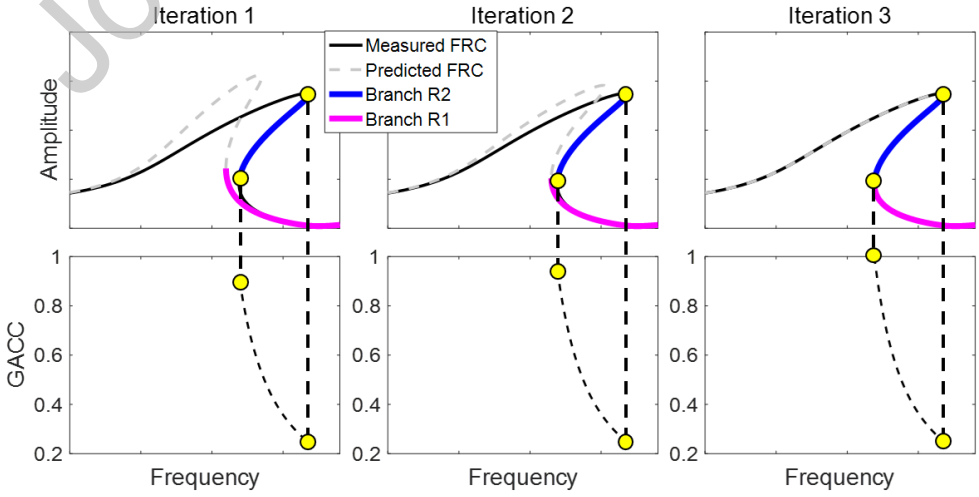

Fig. 14 Schematic diagram of correlation functions between stable and unstable responses

The remaining thick lines of Parts 1 and 3 may contain real correlation functions, which are therefore possibly real. For Part 3, the extraction of real correlations from the possible real correlation functions is schematically shown in Fig. 15. The selection of the real correlation functions is conducted for each column of the map. All possible real correlation functions for a column are plotted together in one figure and the selection is performed at each frequency of the figure. At frequency ω, multiple possibly real correlation functions may exist. The real correlation function is selected from the maximum of the functions, if the maximum is larger than a given threshold. Thus

$$\begin{aligned} &\boldsymbol{\gamma}_\omega = \{\gamma_1 \quad \cdots \quad \gamma_l\}^T \quad \gamma_{\max} = \max(\boldsymbol{\gamma}_\omega) \\ &\gamma_{real} = \gamma_{\max} \quad if: \gamma_{\max} > T \end{aligned} \tag{15}$$

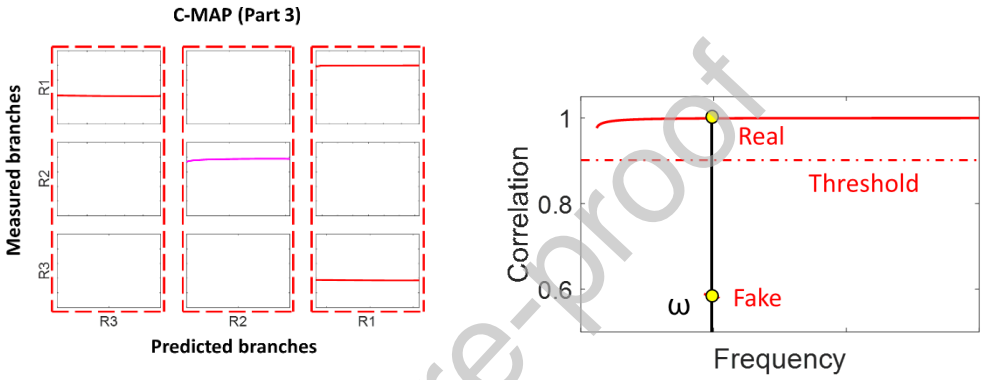

(a) C-MAP (Part 3) (b) Real correlation selection (Column R1)

Fig. 15 Schematic diagram of the extraction of real correlation functions from Part 3

The same selection is also performed on Part 1 for the extraction of the real correlation characteristics. Finally, the selected real GACCs are given in Fig. 16(a). On the FRC plot, the predicted and measured responses that form the real correlation functions are used to establish matched pairs:

$$\begin{array}{ccc} \boldsymbol{X}_{predict}^{real} & & \boldsymbol{X}_{predict}^{real} \\ \downarrow & & \updownarrow \\ \left\langle \gamma_s^{real}, \gamma_a^{real} \right\rangle & \rightarrow & \\ \uparrow & & \boldsymbol{X}_{measure}^{real} \\ \boldsymbol{X}_{measure}^{real} & & \end{array} \quad matched \tag{16}$$

The response matching between the predicted and measured FRCs can then be established according to the real multivalued correlation functions at the whole frequencies. Considering the similarity, the matched response pairs show a relatively good mapping relationship between the predicted and measured FRCs. On the correlation plot, the selected real correlations contain high values and only occupy a small discontinuous region of the whole multivalued correlation curve. Then, when the predicted FRC gradually converges to the measured FRC, the variation of the selected real correlations is given in Fig. 16(b). It is clear that the real GACCs gradually converge to 1, when the predicted and measured FRCs are identical, whereas the fake GACCs converge to curves below unity. Hence, the selected real GACCs are correct.

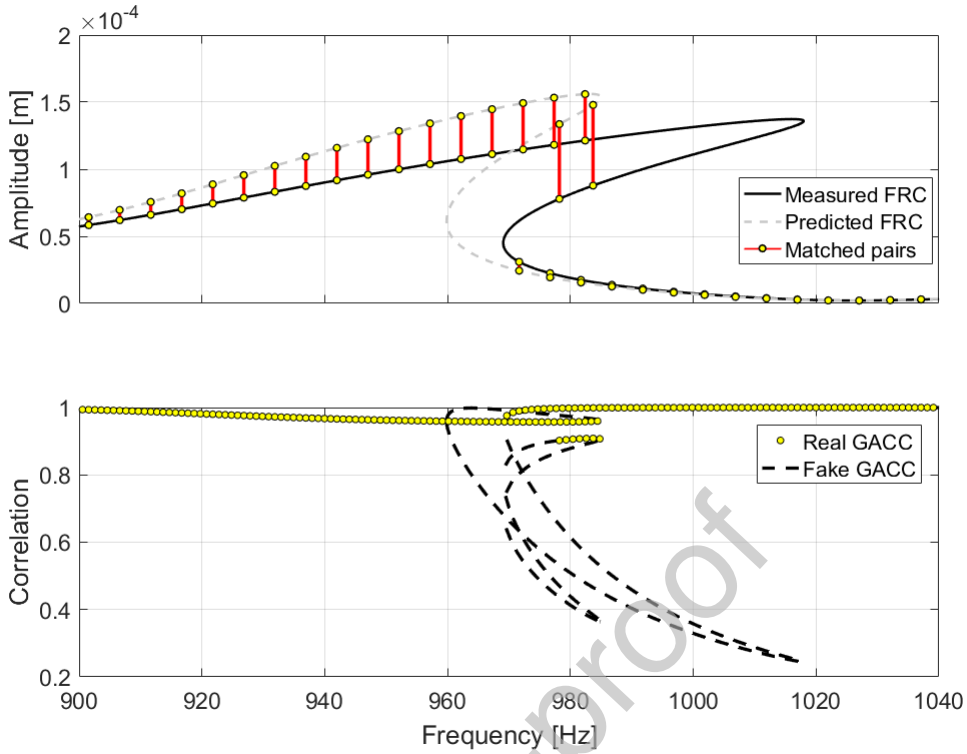

(a) Selected real correlation functions and the related responses

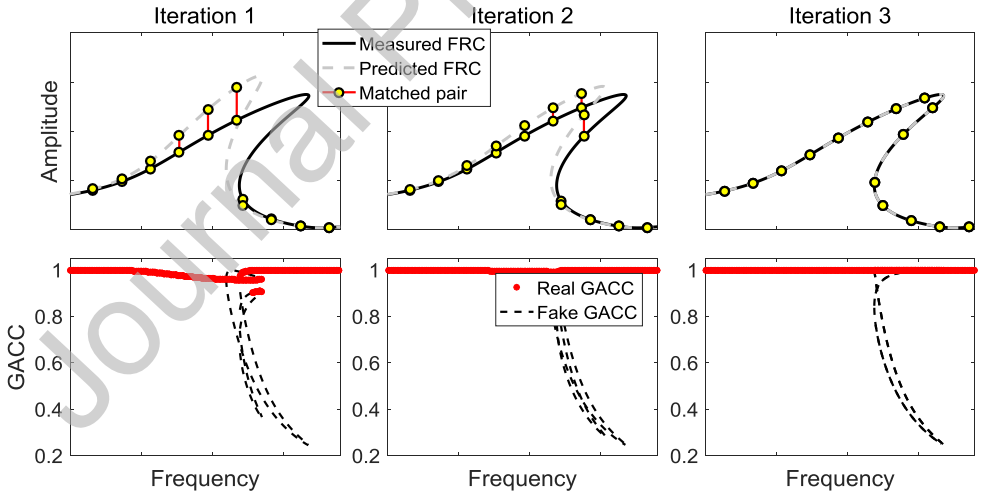

(b) Real correlation functions of FRCs at three iterations

Fig. 16 Schematic diagram of the matched responses and real correlation functions

4 Case study (Ⅰ): correlation analysis of a numerical 3 DOF system with a complex strong nonlinearity

4.1 Simulation of the numerical 3 DOF system with a strong nonlinearity

A 3 DOF system with a strong nonlinearity is simulated to verify the proposed multivalued correlation technique. The equations of motion are

$$\boldsymbol{M}\ddot{\boldsymbol{u}}(t)+\boldsymbol{C}\dot{\boldsymbol{u}}(t)+\boldsymbol{K}\boldsymbol{u}(t)+\sum_{i=1}^{3}k_i^o\times\left(\boldsymbol{N}_i^{ko}\boldsymbol{u}(t)\right)^{\odot p_i^o}=\begin{Bmatrix}0 & F_{ex}\cos(\omega t) & 0\end{Bmatrix}^T$$

$$\boldsymbol{M}=\begin{bmatrix}0.035 & & \\ & 0.035 & \\ & & 0.035\end{bmatrix}\quad \boldsymbol{C}=\begin{bmatrix}20 & -10 & \\ -10 & 20 & -10 \\ & -10 & 10\end{bmatrix}\quad \boldsymbol{K}=\begin{bmatrix}1.2\times10^7 & -8\times10^6 & \\ -8\times10^6 & 1.2\times10^7 & -4\times10^6 \\ & -4\times10^6 & 4\times10^6\end{bmatrix} \tag{17}$$

$$k_1^o=7.2\times10^{14}\left[\mathrm{N/m^3}\right]\quad k_2^o=-8.1\times10^{22}\left[\mathrm{N/m^5}\right]\quad k_2^o=2.5\times10^{30}\left[\mathrm{N/m^7}\right]$$

$$\boldsymbol{N}_1^{ko}=\boldsymbol{N}_2^{ko}=\boldsymbol{N}_3^{ko}=\begin{bmatrix}1 & 0 & 0\\ 0 & 0 & 0\\ 0 & 0 & 0\end{bmatrix}\quad p_1^o=3\quad p_2^o=5\quad p_3^o=7$$

The model has three linear modal frequencies at 830.82Hz, 2176.69Hz and 3851.75Hz. Three polynomial connections are located between DOF 1 and the base, and their values define a complex hardening-softening-hardening property. The system response is predicted using Multi-Harmonic Balance Method (MHBM)-based swept frequency continuation, with the parameters given in Table. 1. The response prediction covers all 3 modes and shows both weak and strong nonlinear responses. The response prediction is simulated and the fundamental harmonic FRCs obtained from the prediction are given in Fig. 17.

Table. 1 Parameters of the MHBM-continuation process

Force [N]	Frequency [Hz]	Max arclength	Initial arclength	Extended harmonics
[0.1~150]	[500,4500]	0.02	0.02	3

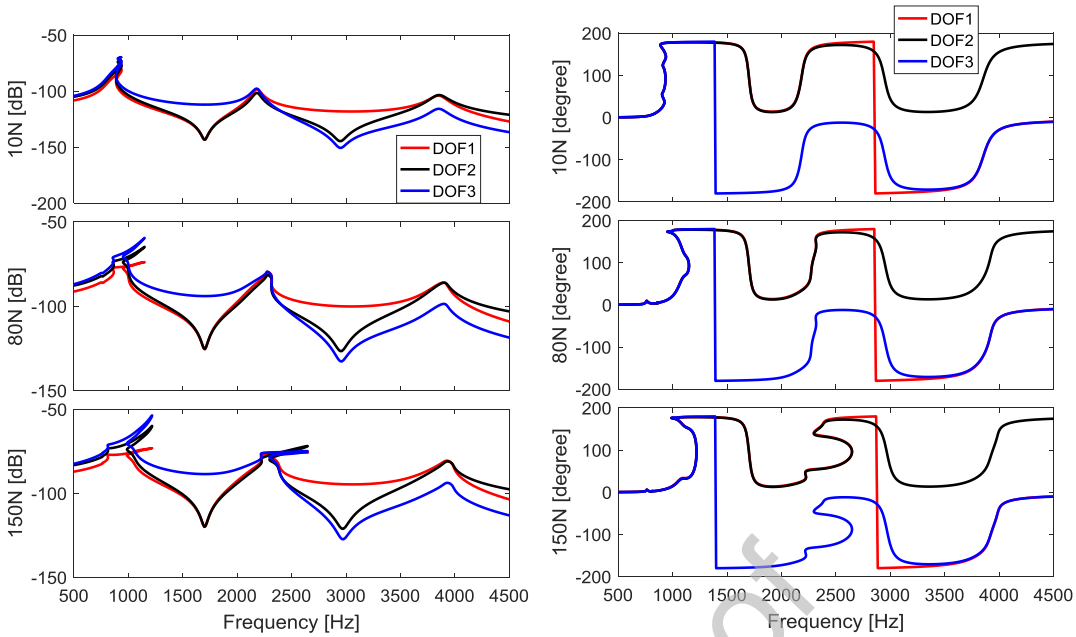

(a) Amplitudes of the 3 DOF multivalued FRC (b) Phases of the 3 DOF multivalued FRC

Fig. 17 Simulated 3 DOF FRCs of the numerical system

Fig. 17(a) and (b) give the amplitudes and phases of the 3 DOF FRCs predicted from the system with the assumed strong nonlinearity. The amplitudes for all 3 DOFs are given on a log scale to better show the effect of the variation of the force. The FRC at mode 1 shows complex multivalued phenomenon when the excitation level is low. As the force increases, the shapes of FRCs gradually change and the nonlinear degree of the system increases. Both responses at modes 1 and 2 show strongly nonlinear behavior and are multivalued. The amplitudes of the FRC at 150N are extracted to highlight their multivalued behavior and the result is given in Fig. 18.

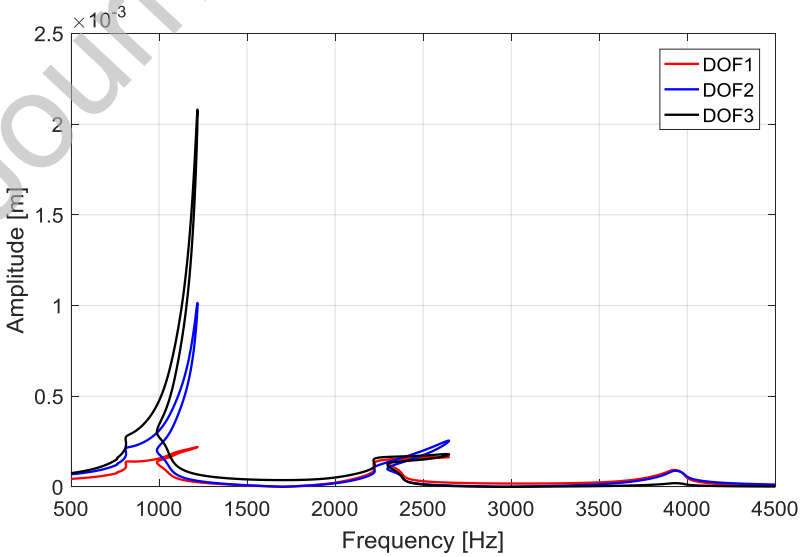

(a) Amplitude (all 3 modes)

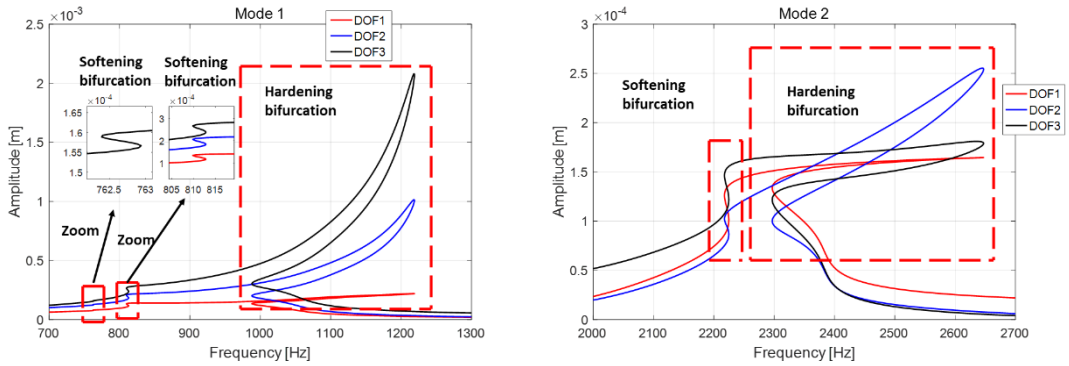

(b) Amplitude (Mode 1) (c) Amplitude (Mode 2)

Fig. 18 Amplitudes of the 3 DOF FRC at 150N

Fig. 18(a) gives the amplitudes of the 3 DOF FRC for all 3 modes. Impacted by the complex nonlinearity, the responses show complex multivalued phenomena in modes 1 and 2. The mode 3 responses do not show any multivalued phenomenon due to high damping. The responses for modes 1 and 2 are zoomed and given in Fig. 18(b) and (c). In mode 1, the response generates a major hardening bifurcation and two small softening bifurcations. In mode 2, the response generates a softening bifurcation and a hardening bifurcation. These phenomena reflect the complex softening-hardening property of the system nonlinearity.

4.2 Computation the multivalued correlation function for the numerical 3 DOF system

The multivalued FRCs at 150N contain clear and complex multivalued phenomenon in both modes 1 and 2. Hence the multivalued responses at 150N are selected as the reference (measured) data for correlation analysis. An initial model is set according to Eq. (17) for the response prediction. The reference and initial models contain the same linear parameters but the nonlinear parameters differ, and these differences are given in Table. 2.

Table. 2 Parameter differences between the initial and reference models

Nonlinear stiffness	$k_1^o\left[\mathrm{N/m^3}\right]$	$k_2^o\left[\mathrm{N/m^5}\right]$	$k_3^o\left[\mathrm{N/m^7}\right]$
Reference	7.2×10^{14}	-8.1×10^{22}	2.5×10^{30}
Initial	7.2×10^{13}	-8.1×10^{21}	2.5×10^{29}

The nonlinear parameters of the initial model are set as 1/10 of the reference nonlinear coefficients, which will reduce the nonlinear strength of the system and change the multivalued behavior of the response. The initial and reference responses are both simulated for comparison. Since the proposed correlation technique is a single nonlinear mode method, the responses from modes 1 to 3 are predicted separately in the frequency bands [500~2000]Hz, [2000~3100]Hz and [3100~4500]Hz. The reference and initial FRCs are overlaid in Fig. 19.

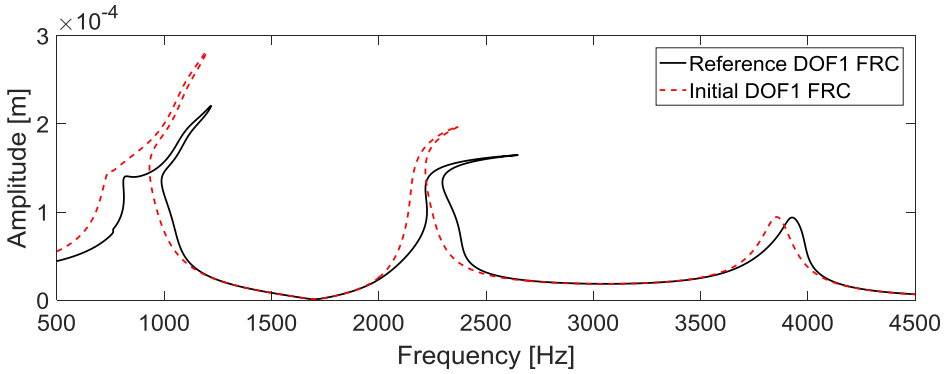

Fig. 19 Overlay between the reference and initial FRCs for all 3 modes

Fig. 19 gives the overlay between the reference and initial FRCs at DOF 1. In mode 1, the softening bifurcation in the reference FRC is not observed in the initial FRC, due to the reduction of the nonlinear coefficients. In mode 2, the initial FRC also does not contain the softening bifurcation, and the reference and initial FRCs show relatively large differences. In mode 3, the variation of the nonlinearity leads to response differences, but does not change the multivalued behavior, since both the reference and initial responses are single-valued. This example will thus demonstrate that the proposed multivalued correlation technique can handle complex multivalued responses with the hardening-softening bifurcations and process FRCs with different multivalued phenomena, but will also quantify differences between single-valued FRCs.

The FRCs for all 3 modes are divided into a set of single-valued branches following the Arclength-based separation method given in Section 3.1, and the separation result for the DOF 1 is given in Fig. 20. The multivalued FRCs of the initial and reference models are separated into single-valued branches with the following labels:

$$\begin{array}{lccc} \textit{Mode} & 1 & 2 & 3 \\ \textit{Reference} & \begin{bmatrix} L1 & L2 & L3 & L4 & L5 \\ & R1 & R2 & R3 & \end{bmatrix} & \begin{bmatrix} L1 & L2 & L3 \\ R1 & R2 & R3 \end{bmatrix} & \begin{bmatrix} L1 \\ R1 \end{bmatrix} \\ \textit{Initial} & \begin{bmatrix} & L1 & \\ R1 & R2 & R3 \end{bmatrix} & \begin{bmatrix} & L1 & \\ R1 & R2 & R3 \end{bmatrix} & \begin{bmatrix} L1 \\ R1 \end{bmatrix} \end{array} \tag{18}$$

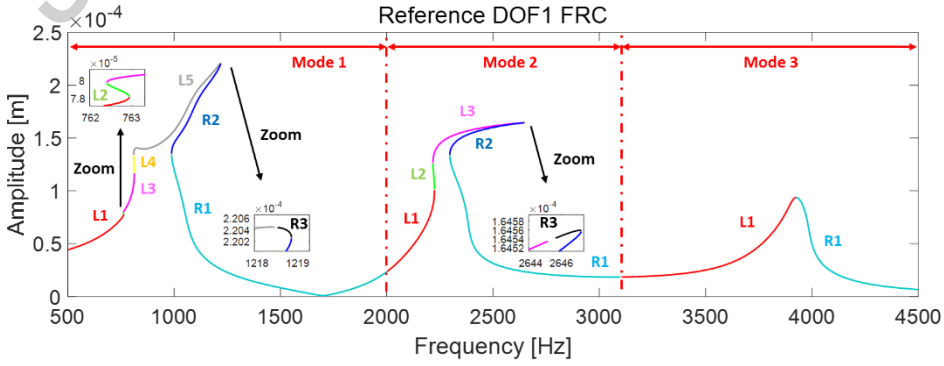

(a) Separation results for the reference DOF 1 FRC

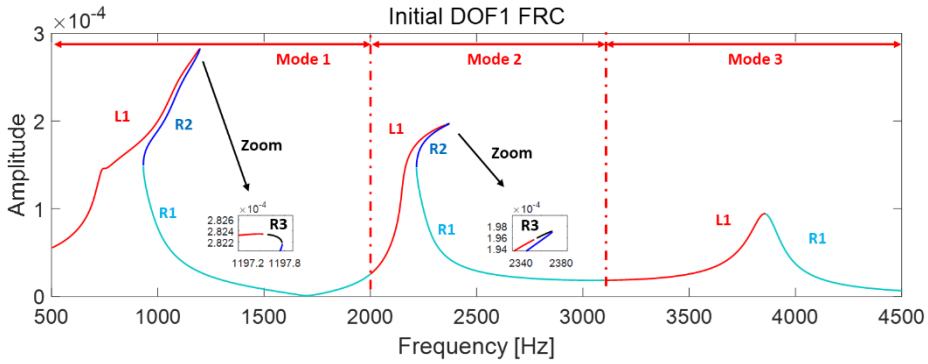

(b) Separation results for the initial DOF1 FRC

Fig. 20 Response separation results for the initial and reference FRCs

The multivalued correlation computation is conducted for the separated branches mode by mode, and the result is given in Fig. 21. In all 3 modes, the shape and amplitude differences between the two 3 DOF FRCs are quantified as scalar curves. For modes 1 and 2, both the GSCC and GACC curves contain complex multivalued phenomena. For mode 3, the correlation curve is single-valued. Hence, both multivalued and single-valued correlation function curves are obtained by the proposed correlation computation technique. For all 3 modes, the correlation functions show that the amplitude differences can better reflect the discrepancies between responses than the shape differences, which may indicate that the GACC is more sensitive than the GSCC for a locally nonlinear structure.

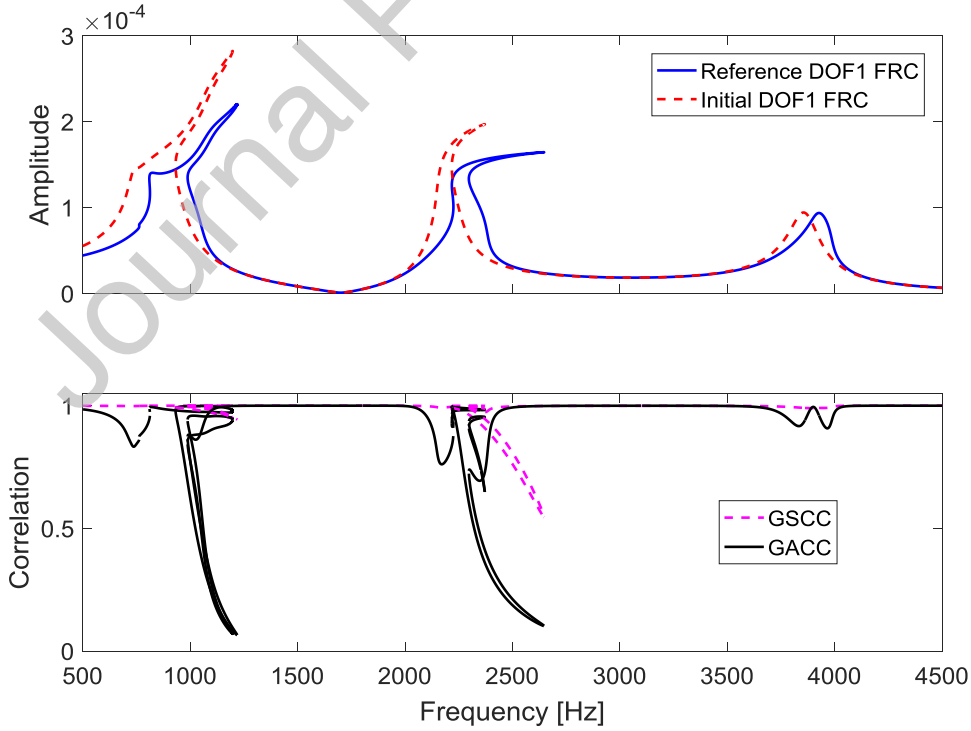

Fig. 21 GSCC and GACC between the 3 DOF FRCs at mode 1

4.3 Multivalued correlation analysis for the numerical 3 DOF system using the C-MAP

After the multivalued correlation function is computed, the real parts should be extracted for accurate correlation analysis. As the GACC shows more sensitivity than the GSCC, the extraction of the real correlation characteristics is conducted based on the GACC. The C-MAP is first extracted from the multivalued GACC and the result is given in Fig. 22.

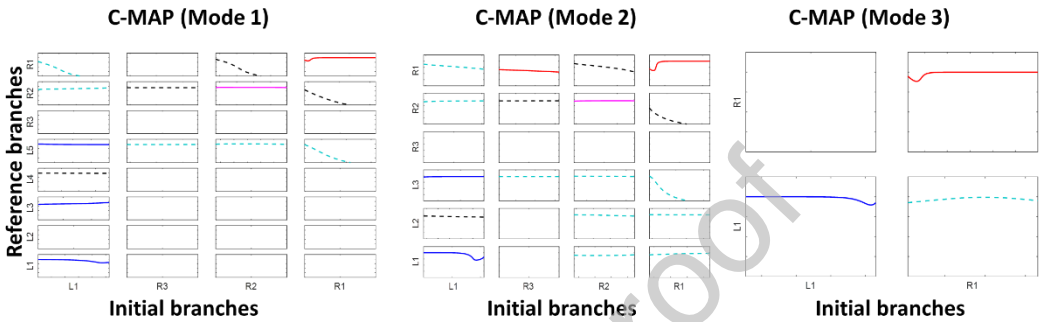

Fig. 22 GACC-based C-MAP between the initial and reference 3 DOF FRCs for all modes

Fig. 22 gives the C-MAPs between the initial and reference FRCs at all 3 modes. As the multivalued phenomena of the FRCs are different at different modes, C-MAPs of the 3 modes are different and the complexity of the C-MAP reduces as the mode number increases. In each of modes 1 and 2, the number of branches of the reference and initial FRCs are different, which reflects differences between the reference and initial multivalued phenomena. In the C-MAP of each mode, the possibly real correlation functions are all marked as thick solid lines and the fake ones are marked as the dotted lines. Real correlation characteristics are then selected from the thick lines of each column. Based on engineering experiences in the traditional linear model updating, the threshold of the selection is set to 0.85 and the result is given in Fig. 23.

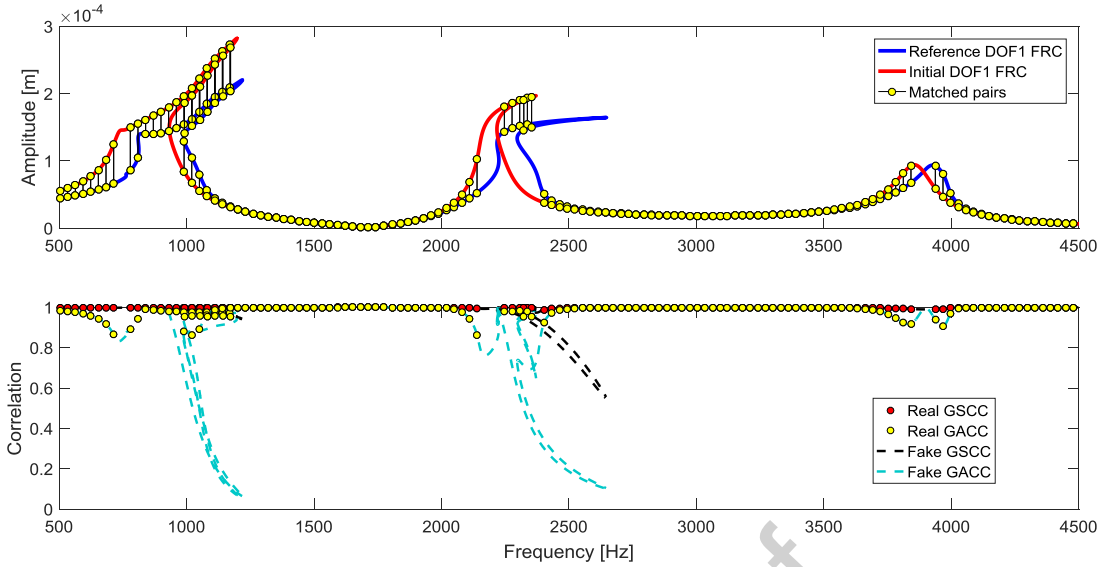

Fig. 23 Selected real correlation characteristics of the numerical 3 DOF system

Fig. 23 gives the selected real correlation characteristics. The C-MAP results in matched response pairs in the FRC plots. Considering the similarity, the matching between the two FRC curves is good. Then, the GSCCs and GACCs between the matched FRC pairs are extracted as the real correlation characteristics, shown in the correlation plot. Similar to Fig. 15, the real correlations are a small part of the whole GSCC and GACC curves. These real correlation characteristics are signed as the output of the proposed multivalued correlation analysis technique and will be used for further correlation-based nonlinear analysis.

Finally, as the nonlinear FRC contains force dependence, the multivalued real correlation functions should also contain the force dependence. When the reference and initial FRCs are fully correlated, the real multivalued GSCCs and GACCs should be the units. Hence, the multivalued global correlation analysis should be further verified. The initial nonlinear model gradually converges to the reference nonlinear model from Iterations 1 to 5:

$$\begin{array}{ccccc} Iteration1 & & \rightarrow & & Iteration5 \\ \boldsymbol{k}_{ini}=10\%\times\boldsymbol{k}_{ref} & & \cdots & & \boldsymbol{k}_{ini}=100\%\times\boldsymbol{k}_{ref} \end{array} \tag{19}$$

At the first iteration, the nonlinear stiffness parameters of the initial model are set as 10% of the reference nonlinear parameters, where the initial FRC varies widely from the reference one. At Iteration 5, the initial nonlinear stiffness parameters are the same as the reference nonlinear parameters. The initial FRC is the same as the reference one. The proposed multivalued correlation analysis is conducted again for the FRCs at Iterations 1 and 5, under three force levels 80N, 150N, 220N. The results are given in Fig. 24.

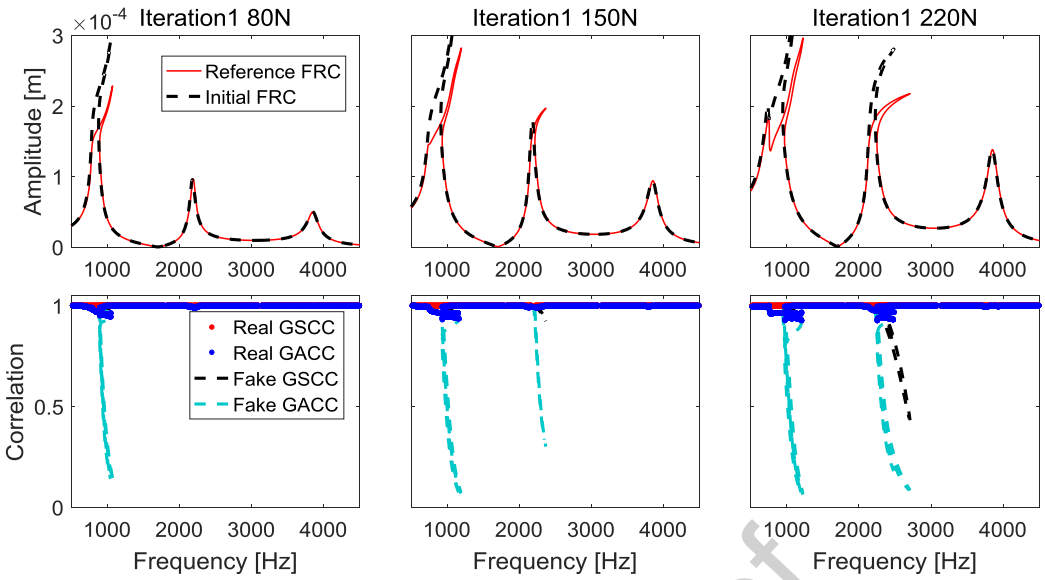

(a) Multivalued global correlation analysis results at Iteration 1

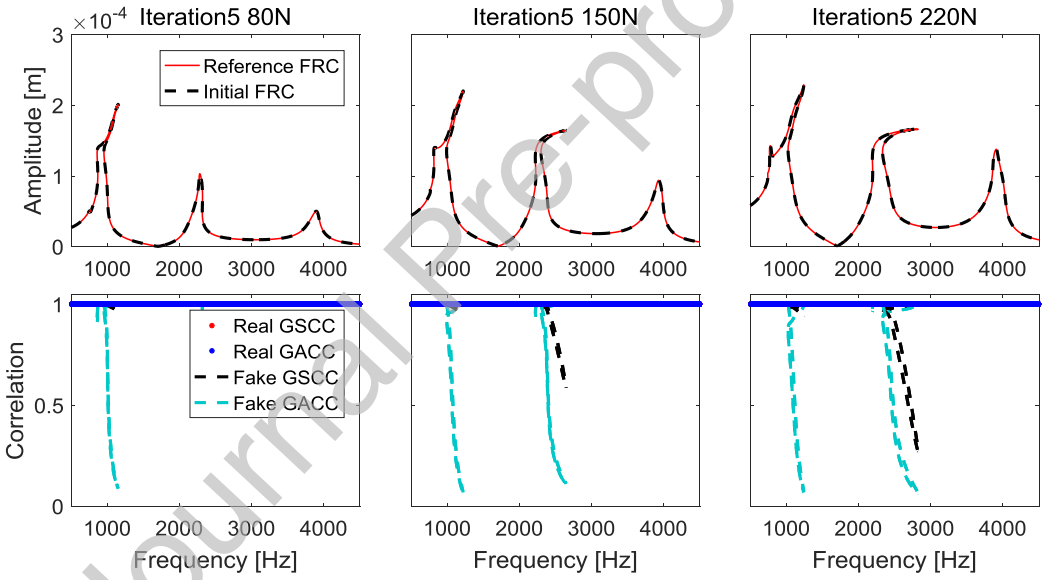

(b) Multivalued global correlation analysis results at Iteration 5

Fig. 24 Multivalued global correlation functions for FRCs at Iterations 1&5

Fig. 24(a) gives the multivalued correlation analysis results at Iteration 1. On the response plot, the initial and reference FRCs change as the force level increases, where the multivalued behavior in these three modes get more complex. Meanwhile, both the real and fake regions of the multivalued correlation function curves get more complex as well with the force increasing. Hence, the variation trends of the multivalued correlation function curves are the same with the FRCs, which verifies its force dependence. Fig. 24(b) gives the multivalued correlation analysis results at Iteration 5. Clearly, on the response plot, the initial and reference FRCs fully coincide with each other, which denote they are fully correlated. Then, for the three force levels, the real regions of the multivalued GSCCs and GACCs all contain the value of 1 and the fake regions are below 1, which shows the real correlation characteristics are successfully selected from the fake ones. The

above results verify the effectiveness of the proposed technique.

5. Case study (Ⅱ): correlation analysis of an experimental 3 DOF structure with a strong nonlinearity

5.1 Test rig and measurement results for the 3 DOF system

An experimental 3 DOF system, shown in Fig. 25, is used to further validate the multivalued correlation technique. Three steel plates act as discrete masses and are joined through four spring-steel plates. Spring plates can be simplified as the linear stiffness and damping connections of the system. There is an arc contact between the base and the spring plates, which is able to provide geometric nonlinear stiffness to the system. Initially, the nonlinear force is smooth and, after the full contact between the spring-plates and the base, the smooth force changes to a non-smooth force. The excitation of the system is provided by a shaker. The applied forces are measured by an impedance head and the responses are measured by accelerometers.

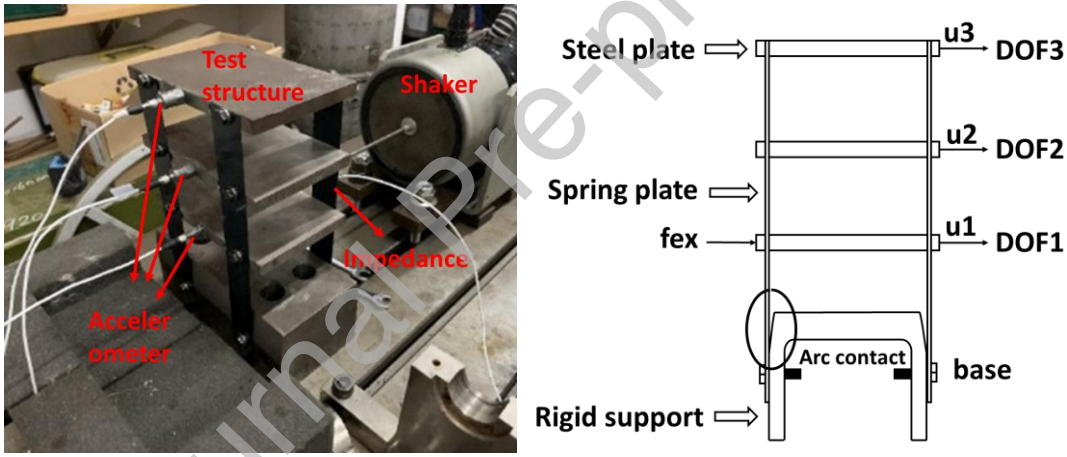

(a) Test rig (b) Nonlinear system

Fig. 25 The experimental 3 DOF structure

A modal test with a low force level is conducted to obtain the linear FRFs from the test rig, and the result is given in Fig. 26(a). The symbol '*dB*' means $20\log_{10}\left(\left(\mathrm{m/s^2}\right)/\mathrm{N}\right)$. The measured responses show modal frequencies of 4.5Hz, 21.88Hz and 36.63Hz. A nominal model was constructed with nominal parameters and updated by the modal test result under the low force level to form the Underlying Linear Model (ULM) of the nonlinear structure. The resulting model is:

$$\boldsymbol{M}_{3\times3}\ddot{\boldsymbol{u}}(t)+\boldsymbol{C}_{3\times3}\dot{\boldsymbol{u}}(t)+\boldsymbol{K}_{3\times3}\boldsymbol{u}(t)=\{f_{ex}\quad 0\quad 0\}^T\cos(\omega t)\quad \boldsymbol{u}(t)=\{u_1(t)\quad u_2(t)\quad u_3(t)\}^T$$
$$\boldsymbol{M}[\mathrm{kg}]=\begin{bmatrix}1.173 & 0 & 0\\ 0 & 1.173 & 0\\ 0 & 0 & 1.173\end{bmatrix}\quad \boldsymbol{C}[\mathrm{N/(m/s)}]=\begin{bmatrix}0.6137 & -0.2958 & 0\\ -0.2958 & 0.3957 & -0.0999\\ 0 & -0.0999 & 0.0999\end{bmatrix} \tag{20}$$
$$\boldsymbol{K}[\mathrm{N/m}]=\begin{bmatrix}23470.13 & -20400 & 0\\ -20400 & 40800 & -20400\\ 0 & -20400 & 20400\end{bmatrix}$$

The linear FRFs were predicted from the ULM and overlaid with the measured FRFs, shown in Fig. 26(b). The measured and predicted curves match well, which verifies the effectiveness of the ULM.

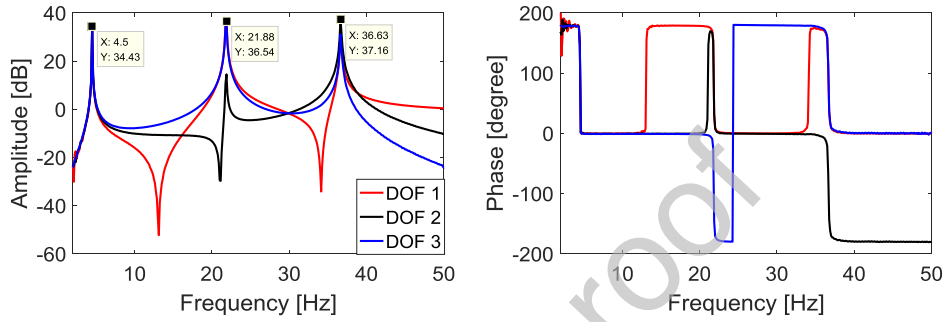

(a) FRFs measured under low force level

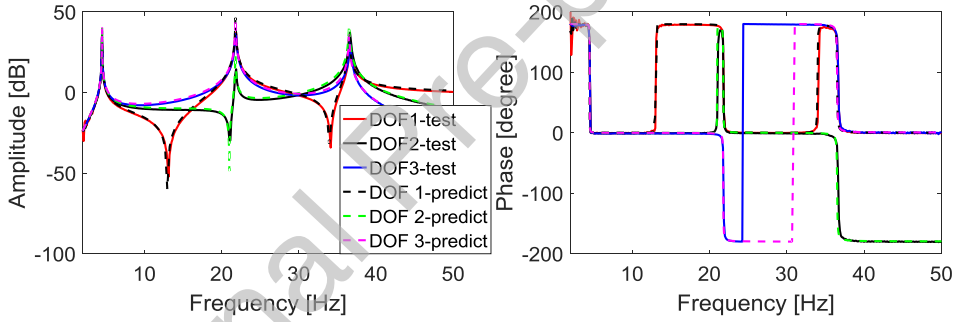

(b) FRFs of the measured and predicted models

Fig. 26 Measured and predicted linear FRFs from the 3 DOF system

The shaker voltage is used as the independent parameter to implement the continuation test at fixed frequencies, to measure the multivalued responses with both stable and unstable regions. The measurement parameters are given in Table. 3 and only responses near mode 1 are measured. The measured amplitudes and phases are given in Fig. 27(a) and (b). For all 3 DOFs, the measured responses contain clear multivalued responses after 4.5Hz.

Table. 3 Parameters of shaker voltage-based fixed frequency continuation

Frequency [Hz]	Voltage [V]	Sampling Frequency [Hz]	Sampling Period [s]
4.45:0.01:5.6	0.02:0.02:2	1000	4

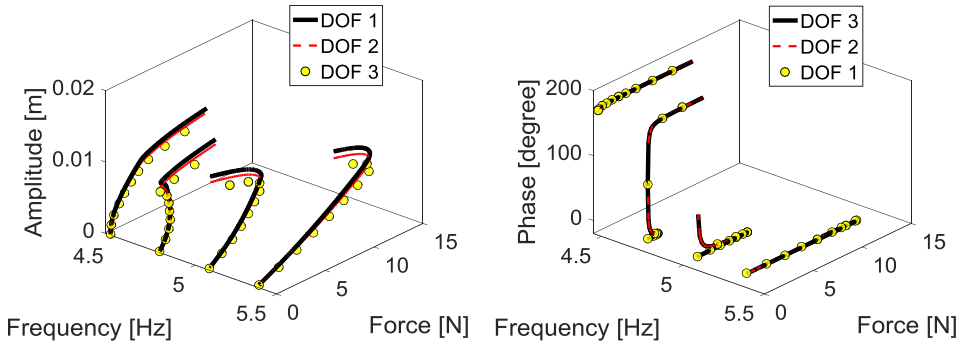

(a) Amplitudes of the fixed frequency test result (b) Phases of the fixed frequency test result

Fig. 27 Measured multivalued Force-Amplitude curves at fixed frequencies

The measurement results at fixed frequencies are then reconstructed as FRCs for the following force levels:

$$[0.05 \quad 0.3 \quad 2]\mathrm{N} \tag{21}$$

The reconstruction results are given in Fig. 28. At 0.05N, the FRC is multivalued and shows a hardening nonlinear behavior. The measured multivalued phenomenon is complete and with both stable and unstable parts. At 0.3N, the reconstructed FRC contains a non-smooth change around 0.008m, which means that the signature of the geometric nonlinearity changes from smooth to non-smooth. At 2N, the non-smooth hardening bifurcation can still be observed on the curve, but the reconstructed curves are missing a major part of the resonance region. The reason is that responses near resonance contain large amplitudes that require large voltage levels and the resulting responses are too large and dangerous to measure.

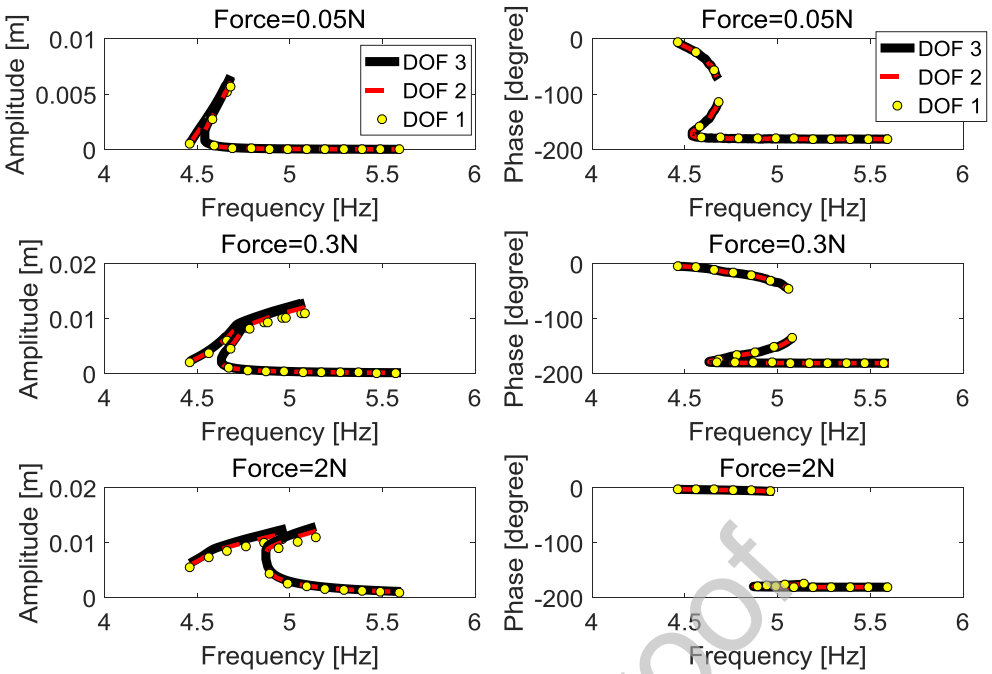

(a) Amplitude of the reconstructed FRCs (b) Phases of the reconstructed FRCs

Fig. 28 Recontructed FRCs at different force levels

5.2 Computation of the multivalued correlation function for the real 3 DOF system

The reconstructed FRC at 0.3N is selected as the reference data for the correlation analysis, as it contains clear non-smooth nonlinear behavior and a multivalued phenomenon that is relatively complete. In our previous research, this curve was used for model updating of a strongly nonlinear model with a 5th order polynomial stiffness. The updated model at iteration 10 is selected as the initial model for the correlation analysis, and the model is:

$$\begin{aligned}
&\boldsymbol{M}_{3\times3}\ddot{\boldsymbol{u}}(t)+\boldsymbol{C}_{3\times3}\dot{\boldsymbol{u}}(t)+\boldsymbol{K}_{3\times3}\boldsymbol{u}(t)\\
&+\sum_{i=1}^{2}k_{odd}^{i}\left(\boldsymbol{N}_{kodd}^{i}\boldsymbol{u}(t)\right)^{\odot 2i+1}+\sum_{i=1}^{2}k_{even}^{i}\left(sign\left(\boldsymbol{N}_{keven}^{i}\boldsymbol{u}(t)\right)\odot\left(\boldsymbol{N}_{keven}^{i}\boldsymbol{u}(t)\right)^{\odot 2i}\right)\\
&=\left\{f_{ex}\quad 0\quad 0\right\}^{T}\cos(\omega t)\\
&\boldsymbol{N}_{kodd}^{i}=\boldsymbol{N}_{keven}^{i}=\begin{bmatrix}1&0&0\\0&0&0\\0&0&0\end{bmatrix},i=1,2\\
&k_{odd}^{1}=3.3324\times10^{7}\left[\mathrm{N/m^3}\right]\quad k_{odd}^{2}=2.4284\times10^{11}\left[\mathrm{N/m^5}\right]\\
&k_{even}^{1}=-1.5618\times10^{4}\left[\mathrm{N/m^2}\right]\quad k_{even}^{2}=-5.3700\times10^{9}\left[\mathrm{N/m^4}\right]
\end{aligned}\tag{22}$$

The model is predicted using the continuation parameters given in Table. 4. The predicted FRC is overlaid on the measured FRC, where the result at DOF 1 is given in Fig. 29.

Table. 4 Parameters of the MHBM-continuation process of the predicted model

Force [N]	Frequency [Hz]	Max arclength	Initial arclength	Extended harmonics
0.3	[4,8]	0.01	0.01	3

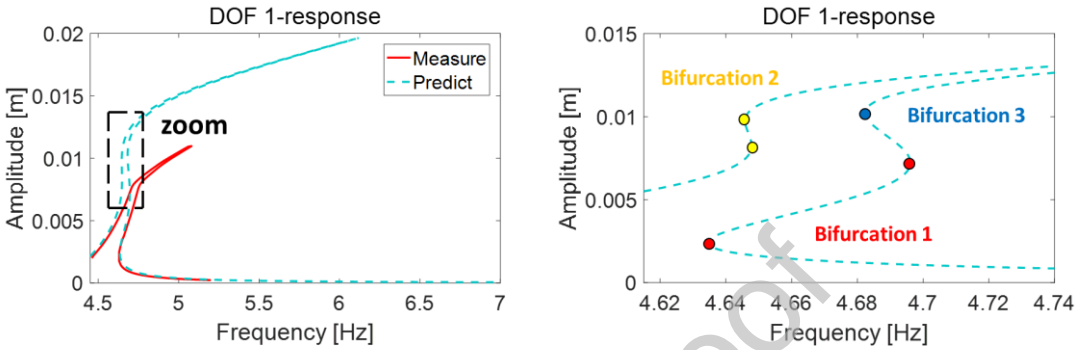

(a) Amplitude (b) Zoom of the black rectangle region in (a)

Fig. 29 Overlay of the measured and predicted FRCs at DOF 1

Fig. 29(a) gives the overlay of the measured and predicted FRCs at DOF 1. To monitor the non-smooth nonlinear behavior of the measurement, the predicted FRC is nearly vertical to the X axle around the black rectangle region and contains complex multivalued behavior. Near the black rectangle, the predicted FRC is zoomed in Fig. 29(b). It is clear that the predicted FRC contains two hardening bifurcations and one softening bifurcation, which shows that the predicted model has a hardening-softening-hardening nonlinearity. The measured FRC only contains the hardening bifurcation, and so the predicted and measured FRCs contain different multivalued behavior.

The predicted and the measured curves are separated using the arclength coordinate for the computation of the multivalued correlation function, where the separated branches at DOF 1 are given in Fig. 30. The predicted FRC is separated into seven single-valued branches and the measured FRC is separated to three branches, and their labels are:

$$\begin{aligned} &Predict: L1 \quad L2 \quad L3 \quad R4 \quad R3 \quad R2 \quad R1 \\ &Meausre: L1 \quad R2 \quad R1 \end{aligned} \tag{23}$$

Single-valued correlation functions are then established between the separated branches of the predicted and measured FRCs, and superposed to form the multivalued correlation function. The results are given in Fig. 31 and Fig. 33.

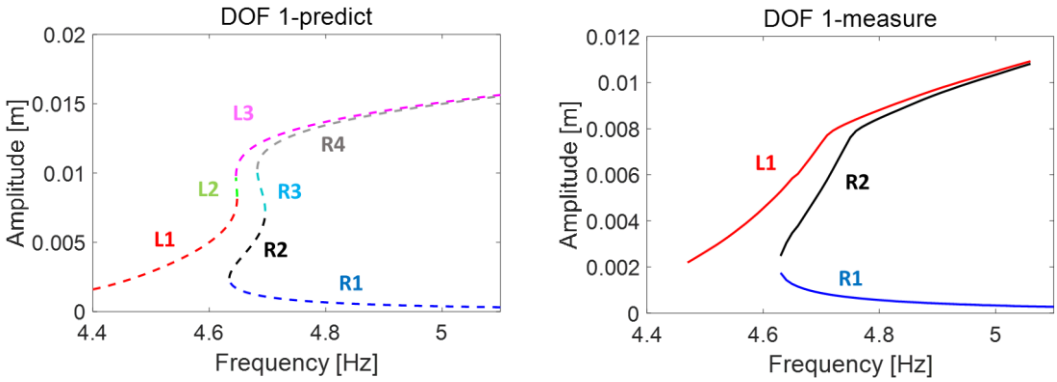

(a) Amplitude (Predict) (b) Amplitude (Measure)

Fig. 30 Arclength-based response separation results of the measurement and prediction

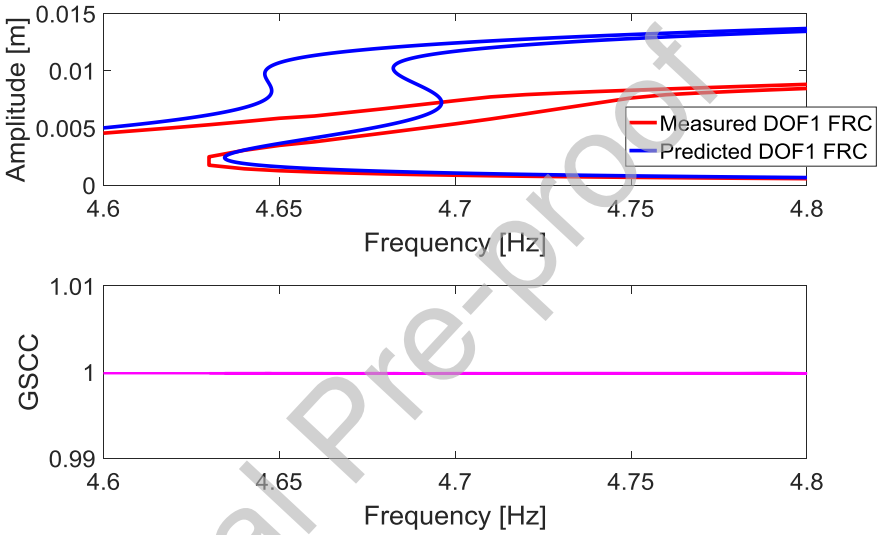

Fig. 31 Multivalued GSCC between the predicted and measured 3 DOF FRCs

The multivalued GSCC of the real 3 DOF system is given in Fig. 31. The shape differences between the predicted and measured FRCs are quantified by the correlation function curve. However, the curve is always equal to 1 and does not show any multivalued phenomenon because of the special location of the nonlinearity. Following Eq. (22), the nonlinear force term is moved from the left side of the equation to the right side:

$$\boldsymbol{M}\ddot{\boldsymbol{u}}+\boldsymbol{C}\dot{\boldsymbol{u}}+\boldsymbol{K}\boldsymbol{u}=\boldsymbol{f}_{ex}-\boldsymbol{f}_{nl}=\begin{Bmatrix} f_{ex}-f_{nl}(u_1) \\ 0 \\ 0 \end{Bmatrix}\approx\begin{Bmatrix} f(u_1)\cos(\omega t) \\ 0 \\ 0 \end{Bmatrix} \tag{24}$$

As both the excitation and the nonlinear force are located at DOF 1, the combination of the nonlinear force and the excitation only depends on DOF 1. Neglecting higher harmonic terms of the nonlinear forces, the combination of the forces could be simplified as an harmonic force with the fundamental excitation frequency ω. The response shape of such an equation is decided by the linear terms on the left side, which is not impacted by the nonlinearity and the multivalued phenomenon. This property can be easily seen by normalizing the 3 DOF FRCs to give

$$shape = \begin{Bmatrix} A_1 / A_3 \\ A_2 / A_3 \\ A_3 / A_3 \end{Bmatrix} \tag{25}$$

The response curves and the related response shapes obtained from this normalization are given in Fig. 32. Before the normalization, the predicted and measured FRCs show clear multivalued behavior. The curves of the multivalued FRCs and the linear FRF vary widely. However, after the normalization, the multivalued phenomenon nearly disappears. At different frequencies, the shapes of the linear FRFs, the measured FRCs and the predicted FRCs are nearly the same. Therefore, shapes of the FRCs are not changed by the local nonlinearity and shape-based correlation techniques such as the GSCC fail.

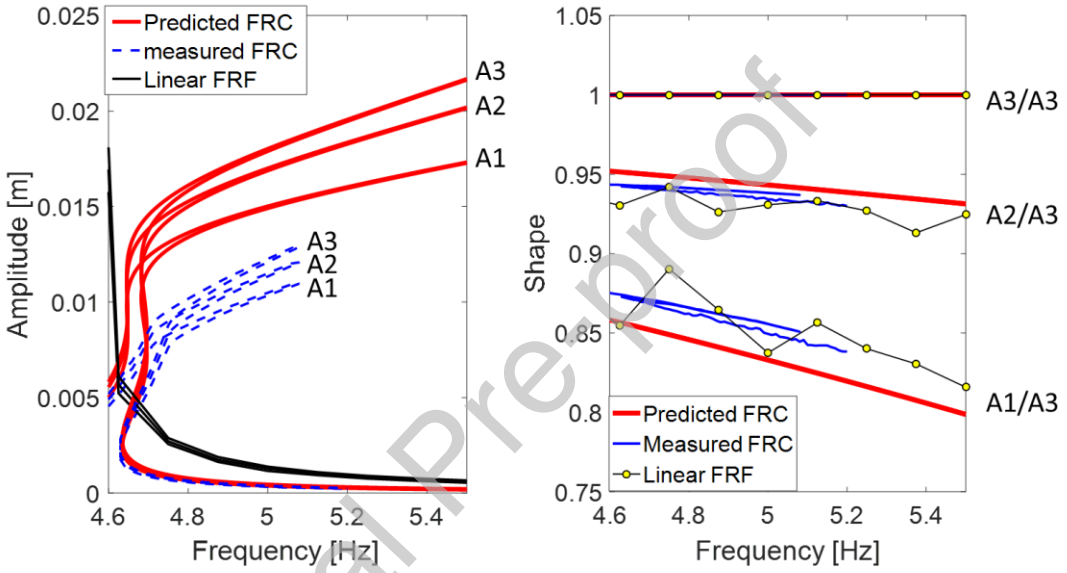

(a) Response curves before the normalization (b) Response shapes after the normalization

Fig. 32 Shapes of nonlinear FRCs and linear FRFs

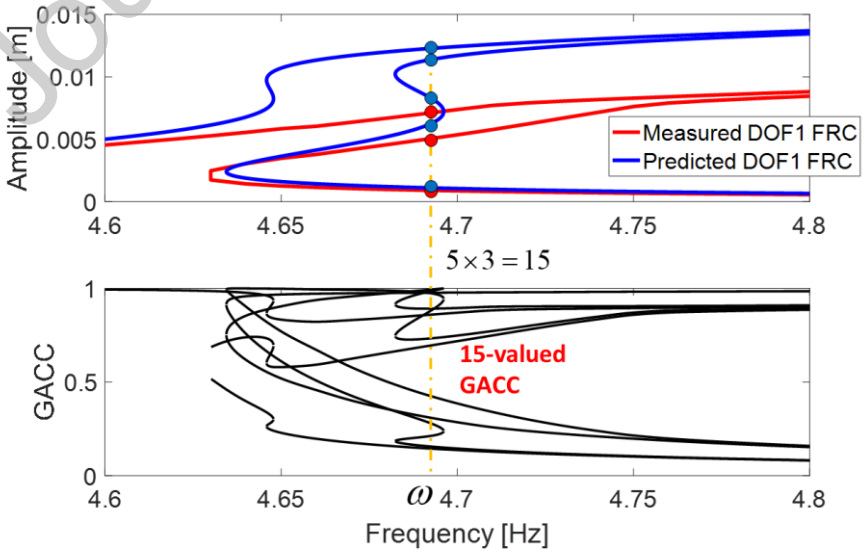

Fig. 33 Multivalued GACC between the measured and predicted 3 DOF FRCs

Fig. 33 gives the multivalued GACC between the multivalued 3 DOF FRCs. Differences between the responses are quantified globally as a scalar curve between 0 and 1, which shows that the global amplitude difference is very sensitive for multivalued FRCs. The multivalued behavior of the predicted FRC frequently varies as the frequency increases, and even has a 5-valued region. As the number of the correlation functions is the product of the numbers of the responses, the 5-valued predicted FRC could induce a 15-valued correlation function with the 3-valued measured FRC. Such a multivalued correlation function is very complex and the number of correlations is 10 larger than the number of responses, which may indicate that many fake correlation functions are within the correlation curve and real correlation selection is required.

5.3 Multivalued correlation analysis for a real 3 DOF system using the C-MAP

As the GSCC is totally insensitive for the experimental 3 DOF system, the real correlation selection is conducted based on the GACC. The C-MAP is first established from the multivalued GACC and the result is given in Fig. 34.

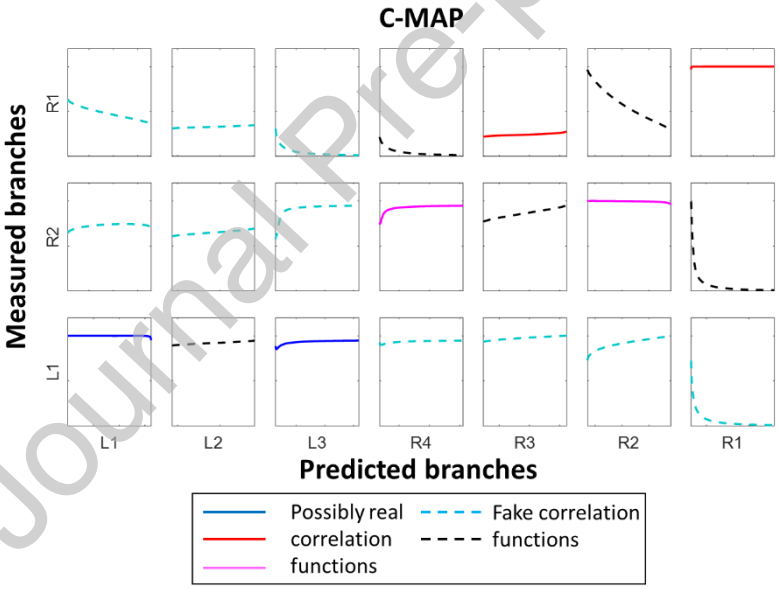

Fig. 34 GACC-based C-MAP of the real 3 DOF structure with a strong nonlinearity

Fig. 34 gives the GACC-based C-MAP between the multivalued 3 DOF FRCs of the measurement and the prediction. The map shows the 21 single-valued correlation functions induced by 7 separated branches of the prediction and 3 separated branches of the measurement. Within the 21 correlation function curves, 6 are possibly real and the remaining 15 curves are fake. Excluding the correlation function curves with the dotted lines, real correlation functions are further selected from the thick lines for each column, where the judgment threshold is set as 0.85. The selection result is given in Fig. 35.

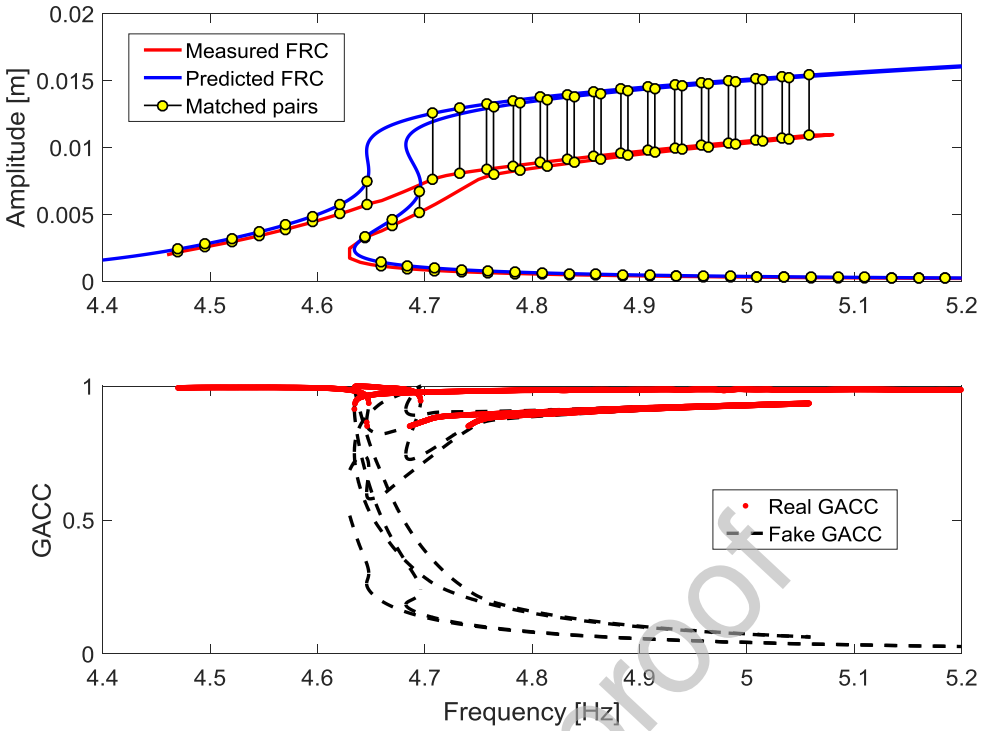

Fig. 35 Matched frequency responses and the related multivalued correlation function

Fig. 35 gives the selected real GACCs between the matched FRC pairs. On the FRC plot, the major region of the predicted FRC with the hardening-softening-hardening bifurcation is matched with the measured FRC with only the hardening bifurcation. Between the matched pairs, real GACCs are established and given in the lower figure. They occupy the high-valued region of the complex 15-valued correlation curve, which are the final output of the multivalued global correlation analysis for the real 3 DOF structure.

Then, the capability of the proposed multivalued global correlation analysis on multiple forces and the correctness of the real correlation selection are validated on the real 3 DOF system. Accordingly, the global correlation analysis is further conducted for the FRCs predicted from the updated models of the real updating Iterations 10 and 18:

$$\begin{aligned} \boldsymbol{k}_{nl}^{iteration,10}: &\quad 0.1\text{N} \quad 0.3\text{N} \quad 2\text{N} \\ \boldsymbol{k}_{nl}^{iteration,18}: &\quad 0.1\text{N} \quad 0.3\text{N} \quad 2\text{N} \end{aligned} \tag{26}$$

Where the updating parameter $\boldsymbol{k}_{nl}^{iteration,10}$ is the nonlinear stiffness vector for the response prediction at Iteration 10 and $\boldsymbol{k}_{nl}^{iteration,18}$ at Iteration 18 in the updating process. $\boldsymbol{k}_{nl}^{iteration,10}$ has been given in Eq. (22). $\boldsymbol{k}_{nl}^{iteration,18}$ is given below:

$$\begin{aligned} k_{odd}^{1} &= 5.7892\times10^{7}\left[\text{N/m}^{3}\right] \quad k_{odd}^{2} = 6.7934\times10^{11}\left[\text{N/m}^{5}\right] \\ k_{even}^{1} &= -4.9165\times10^{4}\left[\text{N/m}^{2}\right] \quad k_{even}^{2} = -1.0895\times10^{10}\left[\text{N/m}^{4}\right] \end{aligned} \tag{27}$$

Multivalued global correlation analysis is then conducted again for the FRCs at both iterations, under three forces, 0.1N, 0.3N and 2N. The results are shown in Fig. 36.

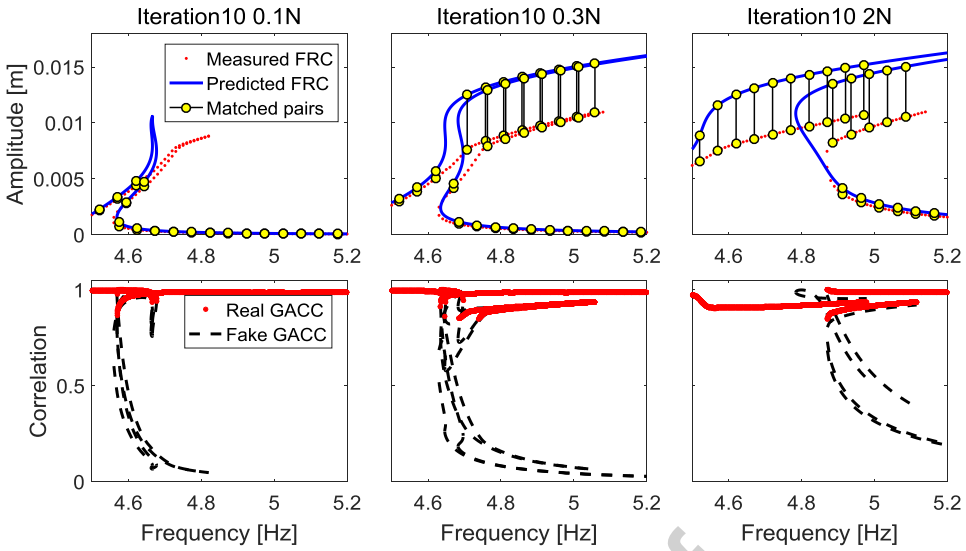

(a) Multivalued global correlation analysis results at Iteration 10

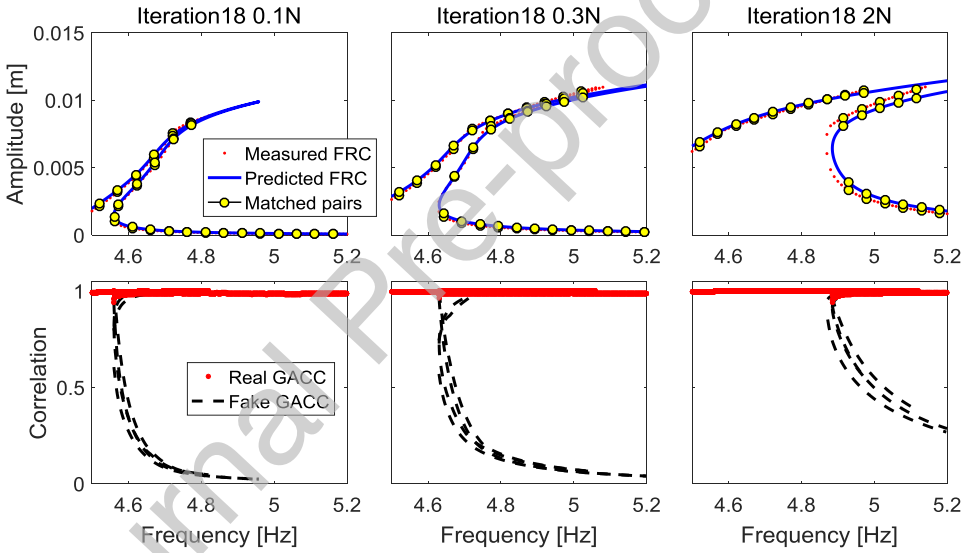

(b) Multivalued global correlation analysis results at Iteration 18

Fig. 36 Global correlation analysis for real FRCs at different force levels

Fig. 36(a) gives the multivalued correlation analysis results of Iteration 10. On the response plot, the predicted FRCs show different multivalued behaviors at three different force levels. Meanwhile, due to the existence of the non-smooth behavior, the response shapes of the measured FRCs at three force levels also show relatively large differences. Even so, under three forces, the matched response pairs corresponding to the selected real GACCs show a good mapping quality between the FRCs, from the view of similarity. On the correlation plot, as the force level increases, the multivalued GACC curves vary widely, which fits the variation trend of the FRC on the response plot. Then, Fig. 36(b) gives the multivalued correlation analysis results of Iteration 18. Clearly, on the response plot, the predicted FRCs nearly coincide with the measured FRCs at the whole 3 forces, which denote the FRCs are nearly fully correlated. At the same time, the multivalued real GACC curves nearly contain the units and the corresponded matched response pairs also shows a good match between the predicted and measured FRCs. These above results

validate the proposed multivalued global correlation analysis technique on the real system.

6. Conclusion

In this paper, the global correlation analysis for strongly nonlinear FRCs with the multivalued phenomenon are proposed, namely the multivalued GSCC and GACC, which are functions of both the frequency and force. Multivalued FRC vectors are first separated into single-valued response branches using the arclength coordinate. The single-valued GSCCs and GACCs are computed as correlation functions between the separated branches of the prediction and measurement, which may be superposed to form the multivalued correlation function. The multivalued correlation function is then represented as the C-MAP and real correlation characteristics are extracted from the map using specific rules. This novel technique has three main advantages: (1) Very complex multivalued correlation functions may be computed. (2) Real correlation characteristics are used for an accurate correlation analysis. (3) Correlation functions are able to quantify the global differences between complex multivalued FRCs with different multivalued behaviors.

The proposed correlation analysis was conducted on a numerical 3 DOF system with a strong nonlinearity for verification. The results show that correlation analysis may be conducted for all 3 modes and the real correlation characteristics were successfully extracted. Furthermore, the GACC is more sensitive than the GSCC on the multivalued FRC. Then, an experimental 3 DOF system was used to further validate the proposed method. Correlation analysis was conducted between the measured FRC with a hardening multivalued phenomenon and the predicted FRC with a hardening-softening-hardening multivalued phenomenon. The two curves generated a 15-valued correlation function, and real correlations were successfully extracted from this complex correlation function using the C-MAP. Global correlation analysis was then successfully conducted at different force levels and real correlations were selected. These show the validity and the superiority of the proposed correlation technique.

The proposed correlation analysis shows great potential to improve the nonlinear analysis approaches, especially for strongly nonlinear systems. Further investigation of applications of the multivalued correlation-based nonlinear analysis, such as model updating and validation, will be investigated and reported in the future.

Acknowledgments

The authors gratefully appreciate the financial support for this work provided by the National Natural Science Foundation of China (12072146) and the National Major Foundational Projects of Aero-engines and Gas Turbines (J2019-I-0008-0008, J2019-IV-0004-0071, J2019-IV-0023-0091). The support of the Jiangsu Province Key Laboratory of Aerospace Power System, the Key Laboratory of Aero-engine Thermal Environment and Structure, Ministry of Industry and Information Technology are also gratefully acknowledged.

Declaration of Competing Interest

The authors declare that they have no known competing financial interests or personal relationships that could have appeared to influence the work reported in this paper.

Reference

[1] Ewins, D.J. (2000) Modal Testing Theory, Practice and Application, 2nd Edition, Research Studies Press, Baldock.

[2] Mottershead, J.E., Link, M. & Friswell, M.I. (2011). The sensitivity method in finite element model updating: A tutorial. Mechanical Systems and Signal Processing, 25, 2275-2296. doi:10.1016/j.ymssp.2010.10.012

[3] Zang, C., Friswell, M.I.. & Imregun, M. (2003). Structural Health Monitoring and Damage Assessment Using Measured FRFs from Multiple Sensors, Part I: The Indicator of Correlation Criteria. doi:10.4028/www.scientific.net/KEM.245-246.131

[4] Zang, C. , Friswell, M.I. & Imregun, M. (2007). Structural health monitoring and damage assessment using frequency response correlation criteria. Journal of Engineering Mechanics, 133(9). doi:10.1061/(ASCE)0733-9399(2007)133:9(981)

[5] Allemang, R.J. & Brown, D.L. (1982). CORRELATION COEFFICIENT FOR MODAL VECTOR ANALYSIS. In Proceedings of the International Modal Analysis Conference & Exhibit (pp. 110–116). Union Coll.

[6] Lieven, N.A.J. & Ewins, D.J. (1988). Spatial correlation of mode shapes: the coordinate modal assurance criterion (COMAC). In Proceedings of the 6th International Modal Analysis Conference (IMAC) (pp. 690–695).

[7] Nefske, D. & Sung, S. (1996). Correlation of a coarse mesh finite element model using structural system identification and a frequency response criterion. In Proceedings of the 14th International Modal Analysis Conference (IMAC).

[8] R. Pascual, J. Golinval & M. Razeto, (1997) A frequency domain correlation technique for model correlation and updating. In Proceedings of the 15th International Modal Analysis Conference (IMAC) (pp. 587–592). .

[9] Zang, C., Grafe, H. & Imregun, M. . (2001). Frequency–domain criteria for correlating and updating dynamic finite element models. Mechanical Systems and Signal Processing, 15(1), 139–155. doi:10.1006/mssp.2000.1357

[10] Rosenberg, R.M. (1960). Normal modes of nonlinear dual-mode systems. Journal of Applied Mechanics, 27(2), 263-268. doi: 10.1115/1.3643948

[11] Rosenberg, R.M. (1966). On nonlinear vibrations of systems with many degrees of freedom. Advances in Applied Mechanics, 9, 155-242. doi: 10.1016/S0065-2156(08)70008-5

[12] Shaw, S.W. & Pierre, C. (1991). Non-linear normal modes and invariant manifolds. Journal of Sound & Vibration, 150(1), 170-173. doi: 10.1016/0022-460x(91)90412-d

[13] Kerschen, G., Peeters, M., Golinval, J.C. & Vakakis, A.F. (2009). Nonlinear normal modes, Part I: A useful framework for the structural dynamicist. Mechanical Systems and Signal Processing, 23(1), 170-194. doi:10.1016/j.ymssp.2008.04.002

[14] Ewins, D.J., Weekes, B. & Delli Carri, A. . (2015). Modal testing for model validation of

structures with discrete nonlinearities. Philosophical Transactions of the Royal Society A Mathematical Physical & Engineering Sciences, 373(2051), 20140410. doi:10.1098/rsta.2014.0410

[15] Taghipour, J., Khodaparast, H.H., Friswell, M.I., Shaw, A.D., Jalali, H. & Jamia, N. (2022). Harmonic-Balance-Based parameter estimation of nonlinear structures in the presence of Multi-Harmonic response and force. Mechanical Systems and Signal Processing, 162. doi:10.1016/j.ymssp.2021.108057

[16] Xie, L., Baguet, S., Prabel, B. & Dufour, R. (2017). Bifurcation tracking by Harmonic Balance Method for performance tuning of nonlinear dynamical systems. Mechanical Systems and Signal Processing, 88, 445-461. doi:10.1016/j.ymssp.2016.09.037

[17] Zhu, T., Zhang, G. & Zang, C. (2022). Frequency-domain nonlinear model updating based on analytical sensitivity and the Multi-Harmonic balance method. Mechanical Systems and Signal Processing, 163. doi:10.1016/j.ymssp.2021.108169

[18] Renson, L., Shaw, A.D., Barton, D.A.W. & Neild, S.A. (2019). Application of control-based continuation to a nonlinear structure with harmonically coupled modes. Mechanical Systems and Signal Processing, 120, 449-464. doi:10.1016/j.ymssp.2018.10.008

[19] Carri, A.D., Weekes, B., Di Maio, D. & Ewins, D.J. (2017). Extending modal testing technology for model validation of engineering structures with sparse nonlinearities: A first case study. Mechanical Systems and Signal Processing, 84, 97-115. doi:10.1016/j.ymssp.2016.04.012

[20] Cooper, S.B., DiMaio, D. & Ewins, D.J. (2018). Integration of system identification and finite element modelling of nonlinear vibrating structures. Mechanical Systems and Signal Processing, 102, 401-430. doi:10.1016/j.ymssp.2017.09.031

[21] Zhu. T, Zhang. G, Zang. C, Cui H, & Friswell. M.I. MSSP-22-1813, Arclength-based response matching of multivalued frequency responses to update models with strong nonlinearities, Mechanical Systems and Signal Processing, revised to be published

CRediT authorship contribution statement

Zhu Tianxu: Conceptualization, Discussion, Methodology, Software, Investigation, Writing – original draft. **Zhang Genbei:** Conceptualization, Discussion **Zang Chaoping:** Conceptualization, Discussion, Investigation, Writing-review & editing, Project administration. **Friswell. M.I**: Conceptualization, Discussion, Writing-review & editing

Declaration of Competing Interest

The authors declare that they have no known competing financial interests or personal relationships that could have appeared to influence the work reported in this paper.